MELT POOL ANALYSIS OF TITANIUM IN SELECTIVE LASER SINTERING USING COMSOL MULTI PHYSICS

A Project report submitted in partial fulfillment of

the requirements for the award of the degree of

BACHELOR OF TECHNOLOGY

In

MECHANICAL ENGINEERING

By

KORADA PAVAN KUMAR	(318126520L19)
GANGADHARANI DINESH	(318126520L20)
SONTHENA AJAY	(317126520118)
SAGARAM CHANDRA VAMSI	(317126520113)
BOMMALI JEEVAN KUMAR	(317126520067)

Under the esteemed guidance of

MR. B S LAKSHMI PRASAD

M.Tech

ANIL NEERUKONDA INSTITUTE OF TECHNOLOGY AND SCIENCES

Autonomous status accorded by UGC and Andhra University

(Approved by AICTE, Permanently Affiliated to Andhra University, Accredited and reaccredited by NBA, accredited by NAAC- 'A' Grade)

Sangivalasa, Bheemunipatnam Mandal

Visakhapatnam (District) – 531162(2017- 2021)

ANIL NEERUKONDA INSTITUE OF TECHNOLOGY & SCIENCES

ANIL NEERUKONDA INSTITUTE OF TECHNOLOGY & SCIENCES (A)

(Affiliated to Andhra University, Approved by AICTE, Accredited by NBA & NAAC with A grade)
SANGIVALASA, VISAKHAPATNAM (District) – 531162

PRAGNANAM BRAHMA
ANITS

CERTIFICATE

This is to certify that the Project Report entitled "**MELT POOL ANALYSIS OF TITANIUM SELECTIVE LASER SINTERING USING COMSOL MULTI PHYSICS**" being submitted by KORADA PAVAN KUMAR (318126520L19), GANGADHARANI DINESH (318126520L20), SAGARAM CHANDRA VAMSI (317126520113), SONTHENA AJAY (317126520118), BOMMALI JEEVAN KUMAR (317126520067) in partial fulfillments for the award of degree of **BACHELOR OF TECHNOLOGY** in **MECHANICAL ENGINEERING, ANITS**. It is the work of bona-fide, carried out under the guidance and supervision of **MR.B.S.LAKSHMI PRASAD**, Assistant Professor, Department Of Mechanical Engineering, ANITS during the academic year of 2017-2021.

PROJECT GUIDE

(MR.B.S.LAKSHMI PRASAD)
Assistant Professor
Mechanical Engineering Department
ANITS, Visakhapatnam.

Approved By

HEAD OF THE DEPARTMENT

(Dr. B. Naga Raju)
Head of the Department
Mechanical Engineering Department
ANITS, Visakhapatnam.

PROFESSOR & HEAD
Department of Mechanical Engineering
ANIL NEERUKONDA INSTITUTE OF TECHNOLOGY & SCIENCES
Sangivalasa-531 162 VISAKHAPATNAM Dist A P

TABLE OF CONTENTS

ABSTRACT

It is known that Titanium alloys are widely used in a variety of industries such as aerospace, automative and biomedical. Good corrosion resistance and the high strength/weight ratio are among the properties that have made these alloys attractive for above mentioned industries. Although these alloys have been extensively investigated for the past decades ,the growing demand, the high cost and the recent development of additive manufacturing techniques require better understanding of these alloys as well as the existing relationship between composition, Processing and properties. Additive manufacturing has since become one of the more prominent manufacturing operations over the past years.

The aim of this research is to predict the distribution of temperature, investigation of thermal stresses in the melt pool of fabricated Titanium Grade 9 by Selective Laser Sintering (SLS)through COMSOL Multiphysics software. Throughout the SLS process the heat transfer characteristics of metal powder plays a significant role in maintaining the product quality during 3D printing. Thus, it is crucial to determine thermal behaviour of alloys and it is a significant challenge to accurately determine the large temperature gradient. This research can assist in evaluation of temperature and stresses in a more effective manner.

The obtained set of equations coupled through the temperature variable was solved using COMSOL Multiphysics. The results are presented in TITANIUM GRADE9 was used, allowing validation of the model. Finally, variations at the melt pool geometry in terms of the operational parameters are analyzed. This model aims at estimation of melt pool temperature and thermal stress distribution during laser powder deposition in time reasonably short to allow for predictable process control.

CHAPTER 1

INTRODUCTION

1.1 ADDITIVE MANUFACTURING:

Additive manufacturing uses data computer-aided-design (CAD) software or 3D object scanners to direct hardware to deposit material, layer upon layer, in precise geometric shapes. As its name implies, additive manufacturing adds material to create an object. By contrast, when you create an object by traditional means, it is often necessary to remove material through milling, machining, carving, shaping or other means.

Although the terms "3D printing" and "rapid prototyping" are casually used to discuss additive manufacturing, each process is actually a subset of additive manufacturing.While additive manufacturing seems new to many, it has actually been around for several decades.

There are a variety of different additive manufacturing processes:

1.1.1 Powder Bed Fusion

Powder Bed Fusion (PBF) technology is used in a variety of AM processes, including direct metal laser sintering (DMLS), selective laser sintering (SLS), selective heat sintering (SHS), electron beam melting (EBM) and direct metal laser melting (DMLM). These systems use lasers, electron beams or thermal print heads to melt or partially melt ultra-fine layers of material in a three-dimensional space. As the process concludes, excess powder is blasted away from the object.

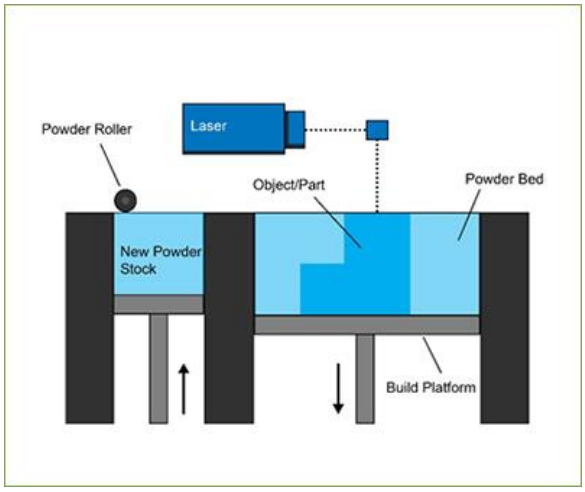

Figure.1.1.1 Powder Bed Fusion

1.1.2 Binder Jetting

The binder jetting process is similar to material jetting, except that the print head lays down alternate layers of powdered material and a liquid binder.

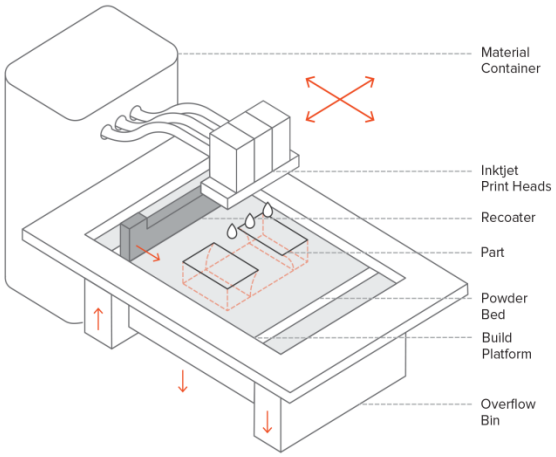

Figure.1.1.2 Binder Jetting

1.1.3 Directed Energy Deposition

The process of directed energy deposition (DED) is similar to material extrusion, although it can be used with a wider variety of materials, including polymers, ceramics and metals. An electron beam gun or laser mounted on a four- or five-axis arm melts either wire or filament feedstock or powder.

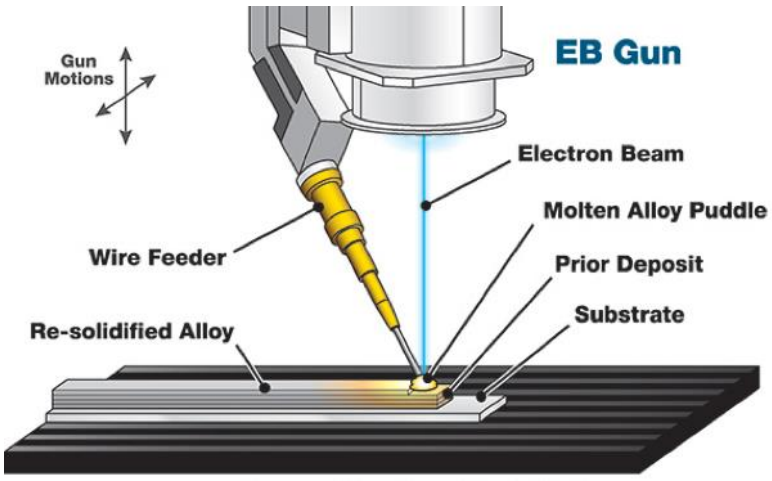

Figure.1.1.3 Directed Energy Deposition

1.1.4 Material Extrusion

Material extrusion is one of the most well-known additive manufacturing processes. Spooled polymers are extruded, or drawn through a heated nozzle mounted on a movable arm. The nozzle moves horizontally while the bed moves vertically, allowing the melted material to be built layer after layer. Proper adhesion between layers occurs through precise temperature control or the use of chemical bonding agents.

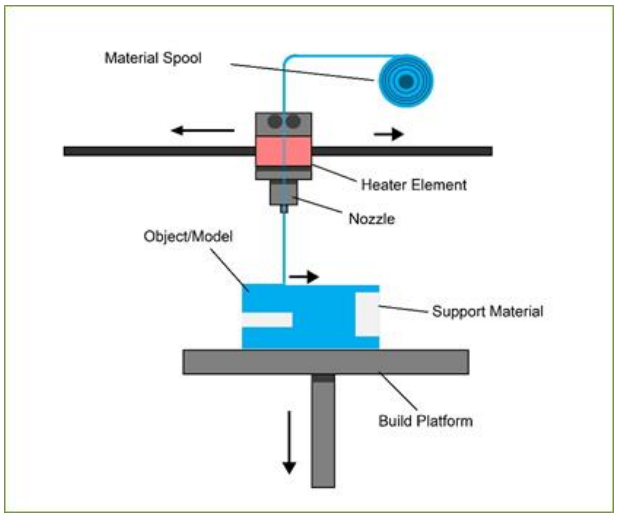

Figure.1.1.4 Material Extrusion

1.1.5 Material Jetting

With material jetting, a print head moves back and forth, much like the head on a 2D inkjet printer. However, it typically moves on x-, y- and z-axes to create 3D objects. Layers harden as they cool or are cured by ultraviolet light.

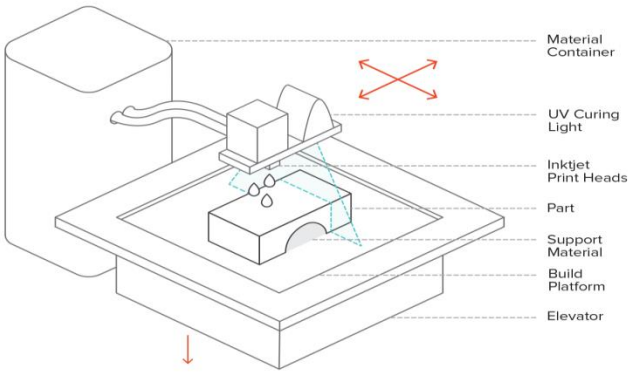

Figure.1.1.5 Material Jetting

1.1.6 Sheet Lamination

Laminated object manufacturing (LOM) and ultrasonic additive manufacturing (UAM) are two sheet lamination methods. LOM uses alternate layers of paper and adhesive, while UAM employs thin metal sheets conjoined through ultrasonic welding. LOM excels at creating objects ideal for visual or aesthetic modelling. UAM is a relatively low-temperature, low-energy process used with various metals, including titanium, stainless steel and aluminium.

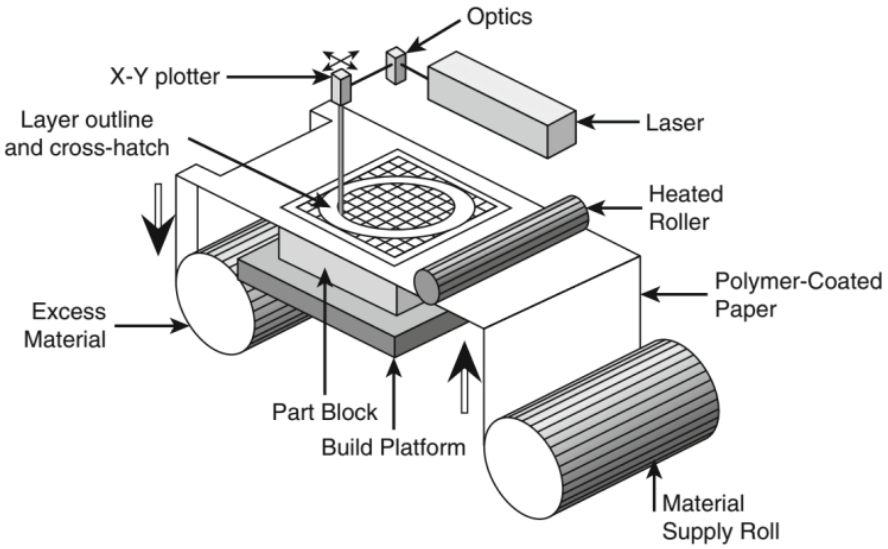

Figure.1.1.6 Sheet Lamination

1.1.7 Vat Polymerization

With vat photopolymerization, an object is created in a vat of a liquid resin photopolymer. A process called photopolymerization cures each microfine resin layer using ultraviolet (UV) light precisely directed by mirrors.

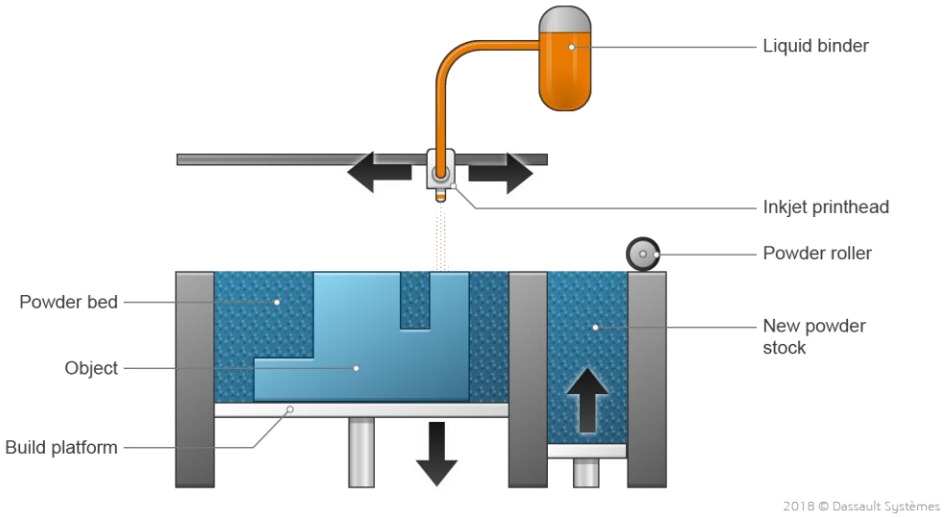

Figure.1.1.7 Vat Polymerization

1.2 ADDITIVE MANFACTURING TECHNOLOGIES:

1.2.1 Sintering

Sintering is the process of creating a solid mass using heat without liquefying it. Sintering is similar to traditional 2D photocopying, where toner is selectively melted to form an image on paper.

1.2.2 Direct Metal Laser Sintering (DMLS)

Within DMLS, a laser sinters each layer of metal powder so that the metal particles adhere to one another. DMLS machines produce high-resolution objects with desirable surface features and required mechanical properties. With SLS, a laser sinters thermoplastic powders to cause particles to adhere to one another.

1.2.3 Direct Metal Laser Melting (DMLM) and Electron Beam Melting (EBM)

By contrast, materials are fully melted in the DMLM and EBM processes. With DMLM, a laser completely melts each layer of metal powder while EBM uses high-power electron beams to melt the metal powder. Both technologies are ideal for manufacturing dense, non-porous objects.

1.2.4 Stereolithography (SLA)

Stereolithography (SLA) uses photopolymerization to print ceramic objects. The process employs a UV laser selectively fired into a vat of photopolymer resin. The

UV-curable resins produce torque-resistant parts that can withstand extreme temperatures.

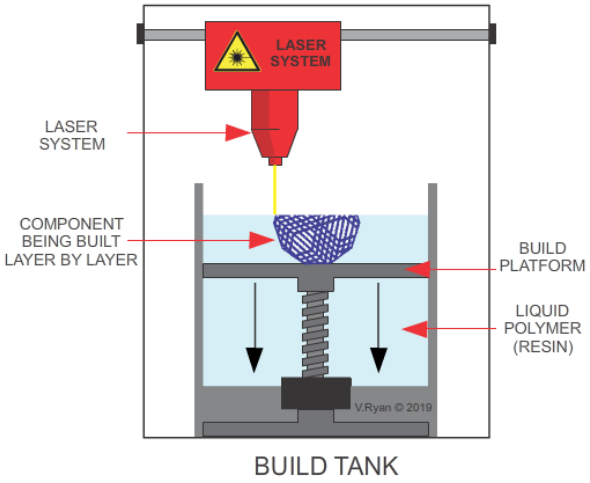

Figure.1.2.1 Stereolithography (SLA)

1.2.5 Selective Laser Sintering:

Selective laser sintering is a powder-based 3D printing technology that uses a laser to fuse material layers into a final part. After the laser traces a cross-section of the CAD design(s) onto a material layer, the build platform lowers and another layer is fused on top. The build platform continues to lower until every layer is built and the part is complete.

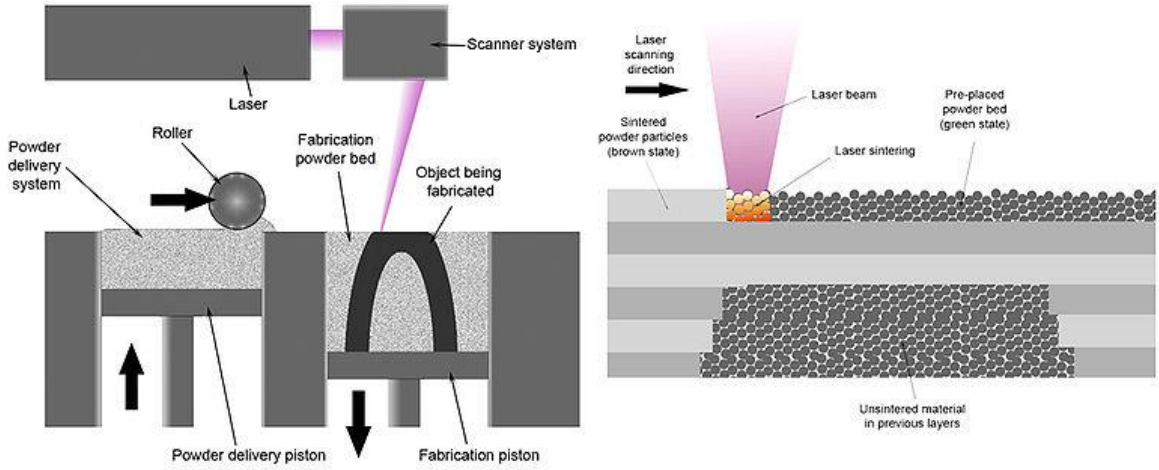

Figure.1.2.2 Selective Laser Sintering

1.2.6 Selective Laser Melting:

Selective laser melting, or SLM, is a type of metal additive manufacturing or 3D printing. Often, the terms SLM and direct metal laser sintering (DMLS) are used

interchangeably. However, the two technologies differ slightly, in that SLM melts pure metals while DMLS fuses metal alloys.

SLM is one of the most exciting 3D printing technologies available today and is utilized both for rapid prototyping and mass production. The range of metal alloys available is fairly extensive. The end result has properties equivalent to those manufactured via traditional manufacturing processes.

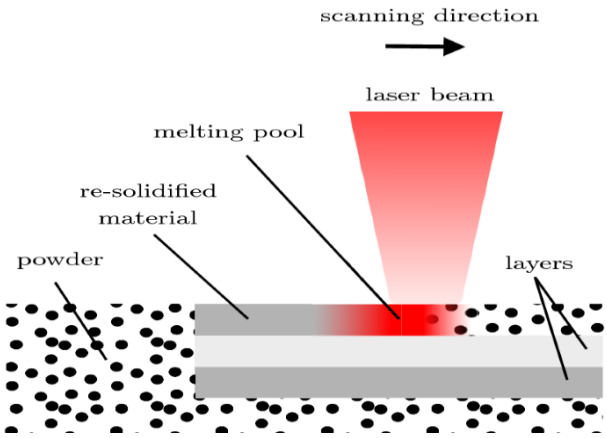

Figure.1.2.3 Selective Laser Melting

1.3 ADDITIVE MANFACTURING MATERIALS:

It is possible to use many different materials to create 3D-printed objects. AM technology fabricates jet engine parts from advanced metal alloys, and it also creates chocolate treats and other food items.

1.3.1 Thermoplastics

Thermoplastic polymers remain the most popular class of additive manufacturing materials. Acrylonitrile butadiene styrene (ABS), polylactic acid (PLA) and polycarbonate (PC) each offer distinct advantages in different applications. Water-soluble polyvinyl alcohol (PVA) is typically used to create temporary support structures, which are later dissolved away.

1.3.2 Metals

Many different metals and metal alloys are used in additive manufacturing, from precious metals like gold and silver to strategic metals like stainless steel and titanium.

1.3.3 Ceramics

A variety of ceramics have also been used in additive manufacturing, including zirconia, alumina and tricalcium phosphate. Also, alternate layers of powdered glass and adhesive are baked together to create entirely new classes of glass products.

1.4 ADDITIVE MANFACTURING ADVANTAGES:

Additive manufacturing allows the creation of lighter, more complex designs that are too difficult or too expensive to build using traditional dies, molds, milling and machining.AM also excels at rapid prototyping. Since the digital-to-digital process eliminates traditional intermediate steps, it is possible to make alterations on the run. When compared to the relative tedium of traditional prototyping, AM offers a more dynamic, design-driven process.

Whether additive manufacturing is used for prototyping or production, lead times are frequently reduced. Lead times for certain jet engine parts have been reduced by a year or more. Also, parts once created from multiple assembled pieces are now fabricated as a single, assembly-free object.

1.5 TITANIUM IN ADDITIVE MANUFACTURING

Titanium has excellent material properties, but its high cost has historically limited its use to high-value applications in aerospace. Now that metal 3D printing is becoming increasingly recognised as a viable manufacturing method, the technology is making titanium more available to industries like medical, automotive and motorsports.

Strong, light and corrosion-proof, and you have the essence of what makes titanium such a sought-after material. Titanium is known for its excellent material properties — as strong as steel but with only 60% of its density.

Titanium’s high strength-to-density ratio, good corrosion resistance and chemical resistance make it particularly desirable for high-performance industries like aerospace and defence.Here, titanium alloys are used in applications that require lightweight parts able to retain their mechanical properties at high temperatures.

1.6 APPLICATIONS OF TITANIUM IN ADDITIVE MANFACTURING

Aerospace dominates the key applications of titanium 3D printing. That said, other industries like medical, motorsports, chemical and marine are also starting to investigate the technology to produce titanium components.

1.6.1 Aerospace

For aerospace companies, 3D printing titanium helps to reduce the weight of highly-loaded structures, making it extremely suitable for jet engines, gas turbines and many airframe components.

1.6.2 Medical

Titanium’s non-toxicity, high strength and resistance to corrosion make it an attractive material for orthopaedic and dental implants.

1.6.3 Automotive & Motorsports Bugatti’s titanium brake caliper

Compared to aerospace and medical, the automotive industry hasn’t been as quick to adopt titanium 3D printing. Even though the same benefits apply, the consumer automotive market is very cost conscious, which limits the use of this expensive material in most vehicles.

1.7 ABOUT TITANIUM GRADE 9

Grade 9 Titanium (3-2.5) is frequently the superior choice for a wide range of applications in industries across the board, perfectly suitable for producing high-tech products ranging from medical pacemakers to aerospace honeycomb.

Titanium Grade 9's mechanical properties offer much more strength than commercially pure titanium. One of the main benefits of this Titanium alloy with 3% Aluminum, 2.5% Vanadium is that it can be cold worked, unlike Ti-6-4,

resulting in good ductility, moderately high strength, and excellent resistance to corrosion.

Ti 3Al-2.5V is the best option for applications where precision is paramount, and helps to reduce our customers' expenses and enhance the JIT (Just in Time) supply chain which is so prevalent in today's competitive tiered manufacturing environment. Versatile grade 9 titanium 3Al-2.5V is available in wire, foil, and strip coils for ordering on-demand with short lead times to reduce the need to stockpile in costly storage facilities.

Grade 9, or TI 3-2.5 titanium for short, can be rolled down to much smaller gauges making it much more versatile for a wider range of parts and components than grade 5. Grade 9 titanium has excellent corrosion resistance and can be used at higher temperatures than the Commercially Pure Grades 1 through 4. Because it can be cold-rolled and formed, Titanium 3-2.5 is ideal for precision applications in the medical, aerospace, marine, and automotive industries with easier workability and excellent corrosion resistance.

1.8 LASER PARAMETERS

1.8.1.Power and Energy (Typical Units: W or J):

The power of a laser is measured in watts (W) and is used to describe either the optical power output of a continuous wave (CW) laser or the average power of a pulsed laser. Pulsed lasers are also characterized by their pulse energy, which is directly proportional to average power and inversely proportional to the laser's repetition rate.Energy is measured in joules (J).

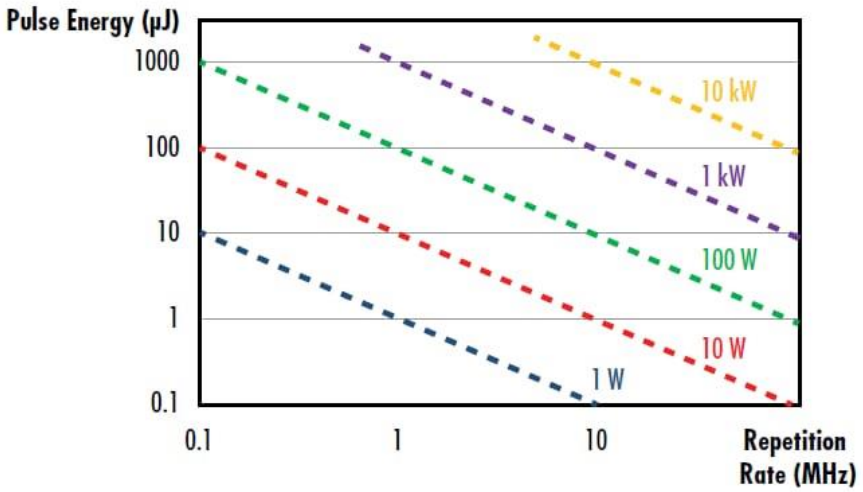

Figure.1.3 Visual representation of the relationship between pulse energy, repetition rate and average power for pulsed lasers

1.8.2.Pulse Duration (Typical Units: fs to ms):

The laser pulse duration, or pulse width, is commonly defined as the full width at half-maximum (FWHM) of the laser's optical power vs. time. Ultrafast lasers, which have numerous benefits for a range of applications including precise materials processing and medical lasers, are characterized by short pulse durations on the order of picoseconds (10-12 s) to attoseconds (10-18 s).

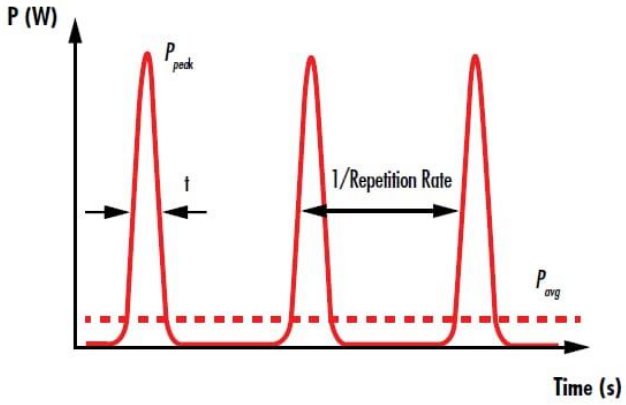

Figure.1.4 The pulses of a pulsed laser are temporally separated by the inverse of the repetition rate

1.8.3.Repetition Rate (Typical Units: Hz to MHz):

A pulsed laser's repetition rate, or pulse repetition frequency, describes the number of pulses emitted every second, or the inverse temporal pulse spacing. As mentioned earlier, repetition rate is inversely proportional to pulse energy and directly proportional to average power. While repetition rate is often dependent on the laser gain medium, in many cases it can be varied. Higher repetition rates result in less thermal relaxation time at the surfaces of the laser optics and at the final focused spot, which leads to more rapid material heating.

1.8.4. Power or Energy Density (Typical Units: W/cm2 to MW/cm2 or µJ/cm2 to J/cm2):

Beam diameter is related to the power/energy density, or the optical power/energy per unit area, of a laser beam. The larger the beam diameter, the smaller the power/energy density of a beam of constant power or energy. High power/energy densities are often ideal at the final output of a system (such as in laser cutting or welding), but low power/energy densities are often beneficial inside a system to prevent laser-induced damage.

1.8.5. Beam Profile:

A laser's beam profile describes the distribution intensity at a cross-section of the beam. Common beam profiles include Gaussian and flat top beams, whose beam profiles follow Gaussian and flat top functions, respectively. However, no laser can produce a perfectly Gaussian or perfectly flat top beam whose beam profile matches its characteristic function perfectly, as there is always some amount of hotspots or fluctuations inside a laser.

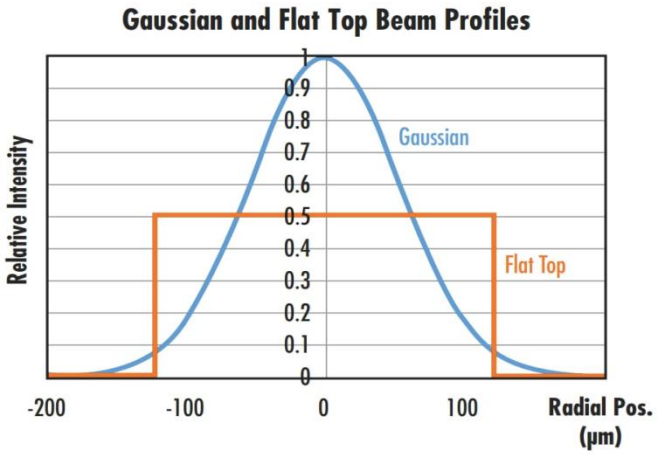

Figure.1.5 A comparison of the beam profiles of Gaussain and flat top beams with the same average power or intensity shows that the Gaussain beam will have a peak intensity 2X that of the flat top beam

1.8.6. Spot Size (Typical Units: µm):

The spot size of a focused laser beam describes the beam diameter at the focal point of a focusing lens system. In many applications, such as materials processing and medical surgery, the goal is to minimize spot size. This maximizes power density and allows for the creation of especially fine features. Aspheric lenses are often used instead of conventional spherical lenses to reduce spherical aberrations and produce smaller focal spot sizes. Some types of laser systems do not end in focusing the laser down to a spot, in which case this parameter is not applicable.

1.8.7. Working Distance (Typical Units: µm to m):

The working distance of a laser system is commonly defined as the physical distance from the final optical element (typically a focusing lens) to the object or surface the laser is focusing onto. Certain applications, such as medical lasers, often seek to minimize working distance, while other applications, such as remote sensing, often aim to maximize their working distance range.

1.8.8. Hatch distance(Typical Units: µm to m):

Scan spacing is the separation between two consecutive laser beams. It is also called hatch spacing or hatch distance.

1.8.9. Scanning speed (Typical Units: mm/s):

The speed is specified in pps (points per second) or kpps (kilo points per second). It describes how fast both mirrors of the scanning system can move and how fast they

can deflect the beam. The higher the scan speed, the better and the smoother the laser beam.

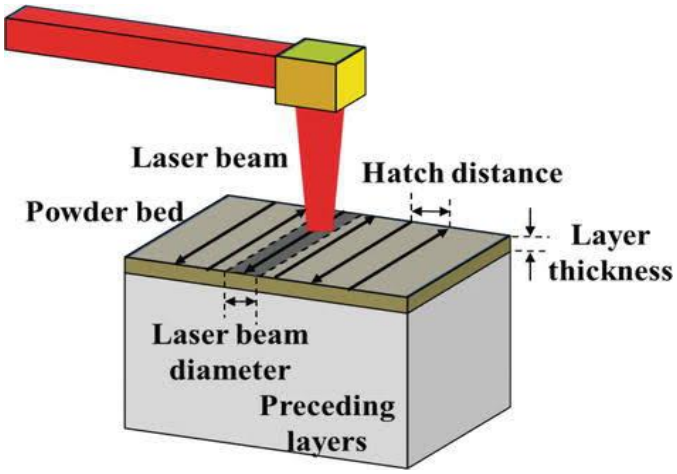

Figure.1.6 Schematic represents all laser parameters

CHAPTER 2

LITERATURE REVIEW

2.1 Temperature measurements during selective laser sintering (SLS) of titanium powder

P.Fischer et al, (2004)

This paper reseraches the comparison of numerical calculations performed with a model for the interaction of near infrared pulses with metallic powders with the temperature measurement obtained using an infrared camera. The average temperature field during continous wave and pulse sintering process are measured. The major findings are the average temperature rises upon continous wave sintering is much higher due to high average power and the camera is not able to resolve the temporarily higher skin temperature in the case of pulsed interaction.

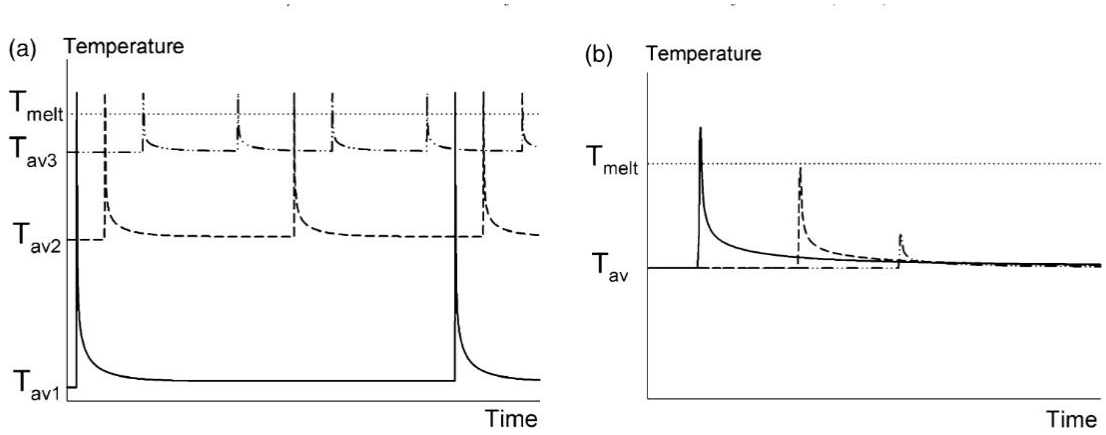

Figure.2.1.1 Melt pool temperature vs time

Schematical depiction of the surface temperature rises (Tskin) upon the interaction at different repetition rates. (a) To overcome the melting temperature, different average temperatures must be achieved at different repetition rates. (b) At a given average power level at different repetition rates, the temperature rise per pulse leads to different sintering: low repetition rate (high energy per pulse, solid line) leads to a good sintering, whereas a high repetition rate (low energy per pulse, dash-dotted line) leads to no sintering at the same average temperature.

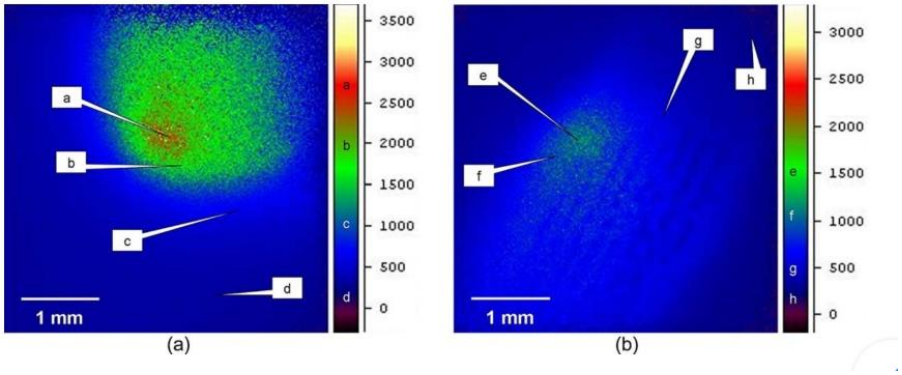

Figure.2.1.2 Measured average temperature field during the (a) continuous wave and (b) pulsed sintering process.

2.2 Computational modelling of laser additive manufactured (LAM) Titanium alloy grade 5

Olawale et al, (2020)

The research of this paper is to study and investigate the influence of temperature distribution and thermal Stresses on the laser additive manfactured Titanium alloy grade 5. The temperature distribution contour was investigated and the influence of parmeters on the final coating geometry. The major findings from this paper are the deposited clad of the composites vaired with change in the selected process parameters which affects the physical. mechanical and metallurgical properties of the composites. Geometrical characteristics of the composites were influenced by the laser power, scan velocity and the powder feed rate.

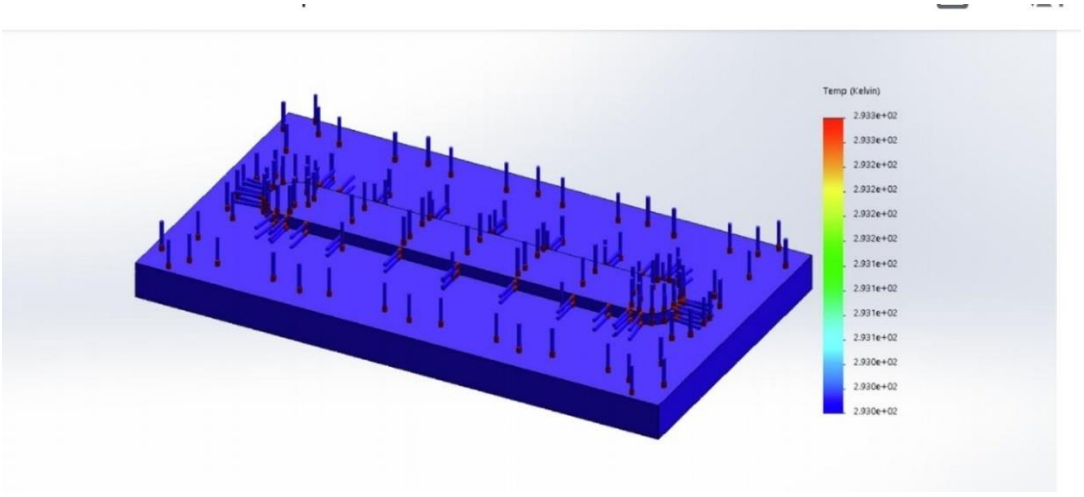

Figure.2.2.1 Temperature distribution on the base alloy at 293 K.

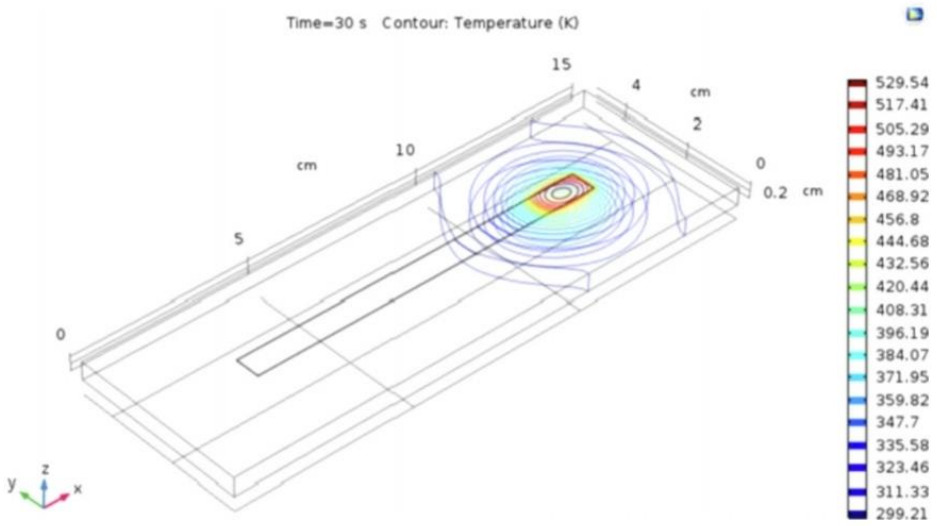

Fig. 5. The shape plot of temperature distribution at the starting point of laser beam.

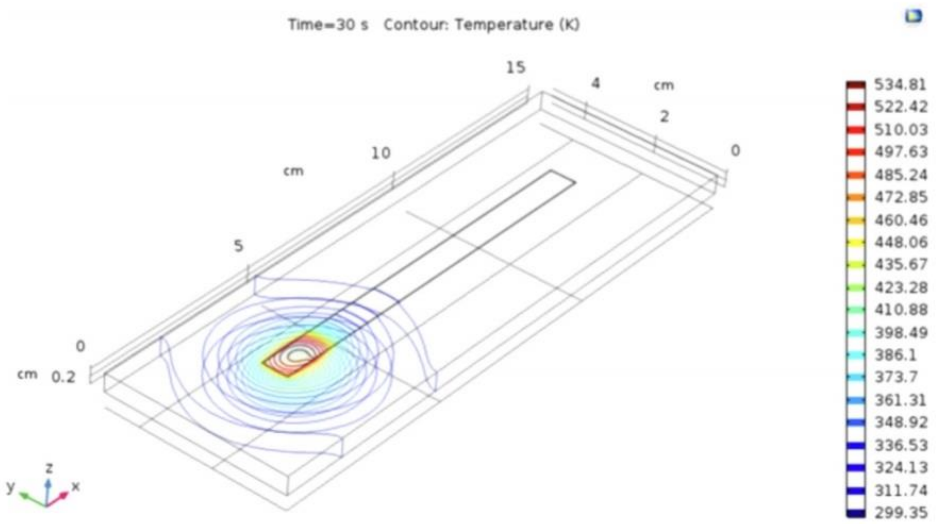

Fig. 6. The shape plot of temperature distribution at the end of the Laser beam.

Figure.2.2.2 Temperature distribution at the starting point of laser beam and at the end of the beam

2.3 The Additive Manufacturing (AM)of Titanium alloys

B.Dutta et al, (2017)

This paper researches one cost effective approach to fabrication of Titanium components. Powder metallurgy technique, Additive manufacturing of Titanium alloy Ti-6Al-4v was discussed. The various approaches to AM are presented. The microstructures and mechanical properties of Titanium alloy are listed. This paper shows the significant advances in AM technologies leading to the production of fully

functional parts using Titanium and its alloys. A major research focus in the AM is dedicated towards process monitoring, control and inline inspection.

2.4 Identification of a suitable volumetric heat source for modelling of selective laser melting of Ti6Al4V powder using numerical and experimental validation approach

Ashish Kumar Mishra et al,(2018)

Using a suitable heat source is crucial to correctly simulate the selective laser melting (SLM) process as the heat source representsthe absorbed heat energy, which governs the thermal and fluid flow phenomena associated with SLM. The discontinuous massdistribution in the powder bed causes absorption of incident laser energy over a substantial depth in the powder bed. Therefore,the conventional way of including laser beam energy as a surface heat flux in the modelling of SLM process is likely to provideinaccurate results. The SLM process involves several physical phenomena such as laser-matter interaction, melting/solidification, conduction-convection-radiation heat transfer and convective fluid flow in the melt pool.

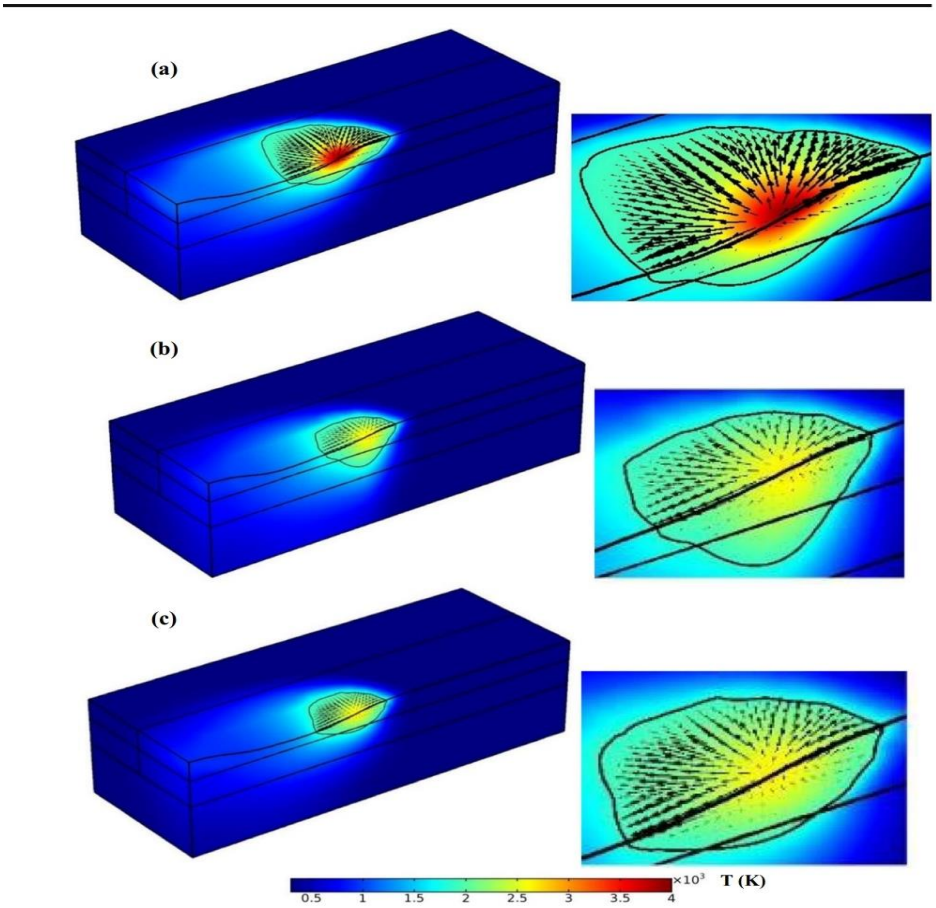

Figure.2.3 Temperature distribution in the computational domain for a surface Gaussian, b Gaussian exponential volumetric and c egg shape volumetric heat source. The magnified view of the melt pool and the velocity field is shown besides each figure

2.5 Temperature profile and melt depth in laser powder bed fusion of Ti-6Al-4V titanium alloy

Luis E. Criales et al, (2017)

In this paper, the prediction of temperatureprofile and melt depth for laser powder bed fusion (L-PBF)of Ti-6Al-4V titanium powder material was performed bynumerically solving the heat conduction-diffusion equationusing a finite difference method. In this paper, a representation of the temperature profileand melt depth in laser fusion of Ti-6Al-4V powdermaterial was obtained. The effect of varying laser pulse energy,average power, and the powder material's density is analyzed. A method to calculate and predict the maximumdepth at which localized melting of the powder materialoccurs is provided.

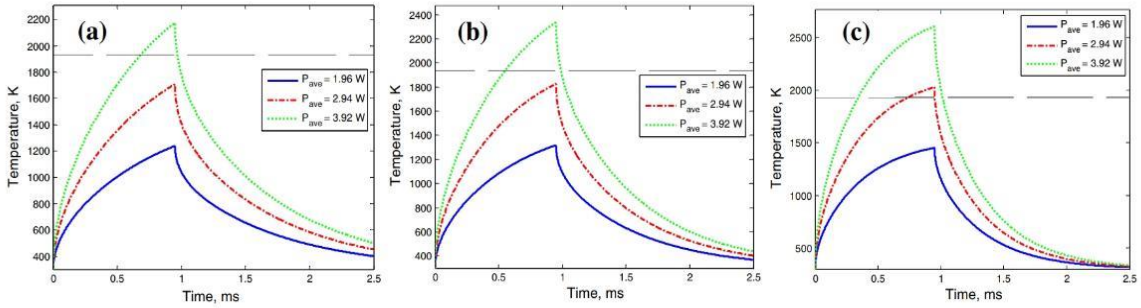

Figure.2.4 Temperature vs. time for a 50% dense, b 40% dense, c 25% dense Ti-6Al-4V by using average intensity as heat source

2.6 Mechanical Properties of Selective Laser Sintering Pure Titanium and Ti-6Al-4V, and Its Anisotropy

Yuu Harada et al, (2020)

This study aimedto investigate the properties of Ti-6Al-4V and pure titanium specimens fabricated using the SLSprocess and compare them with casting specimens. Besides, the effect of the building directionon the properties of the SLS specimens was also investigated. The mechanical properties (tensile strength and elongation),physical properties (surface roughness, contact angle, and Vickers hardness); corrosion resistors (colordifference and corrosion), and surface properties (chemical composition and surface observation)were examined.

The effect of the difference in the building direction of these specimens onthe properties was also investigated. The major findings are that in both metals, the tensile strength of specimens with the same stress direction and buildingdirection was small.For Ti-6Al-4V, the elongation of the specimens molded by SLS (11.27%) was

smaller than thatof the cast specimen (14.72%). In pure Ti, both values were equivalent.

2.7 Selective laser melting of titanium alloy (SLM): investigation of mechanical properties and microstructure

A V Agapovichev et al, (2016)

This article presents the mechanical properties and microstructure of titanium alloy after selective laser melting (SLM). Titanium alloys are ideal material for selective laser melting (SLM), because they are expensive and difficult to machinery using traditional technologies. In this article we focused on the manufacture by SLM and determination of microstructure and mechanical properties of titanium alloy (Ti Grade 2 Powder) using tensile tests and X-ray diffraction. The results reveal that the alloy exhibits a pronounced the homogeneous microstructure and high mechanical strength.The results presented in the paper are the basis of research and development aimed at improving the SLS process and enhances the performance properties of the implants produced. Next important step is the selection of the optimal parameters of selective laser melting and subsequentprocessing as by experimentation and mathematical modeling techniques that will improve and accelerate the process of creating a product with the specified requirements, including the desired roughness of samples

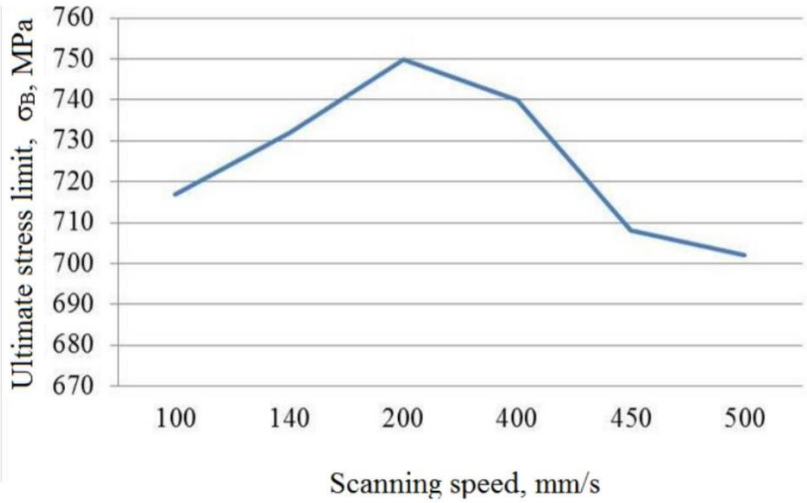

Figure.2.5 The dependence of the mechanical properties of titanium alloy samples VT1-0 from the technological SLM parameters.

2.8 Melt pool sensing and size analysis in laser powder bed metal additive manufacturing.

Bo cheng et al,(2018)

The main objective of this paper is to measure process temperature for selective laser melting (SLM) by using Lumasense MCS640 thermal imager for Inconel 718 material. the process radiant temperature information was collected and speedeffect on melt pool dimension has been investigated. The major findings are that the obtained melt pool length and width has no clear relationship with change of build height, consistentmelt pool dimensions for different speed cases have been observed throughout the build.

Melt pool width would decrease with the increase of scanning speedwhile the trend for length is unclear. Similar melt pool length sizeswere observed at different scanning speeds under a laser power of180 W.

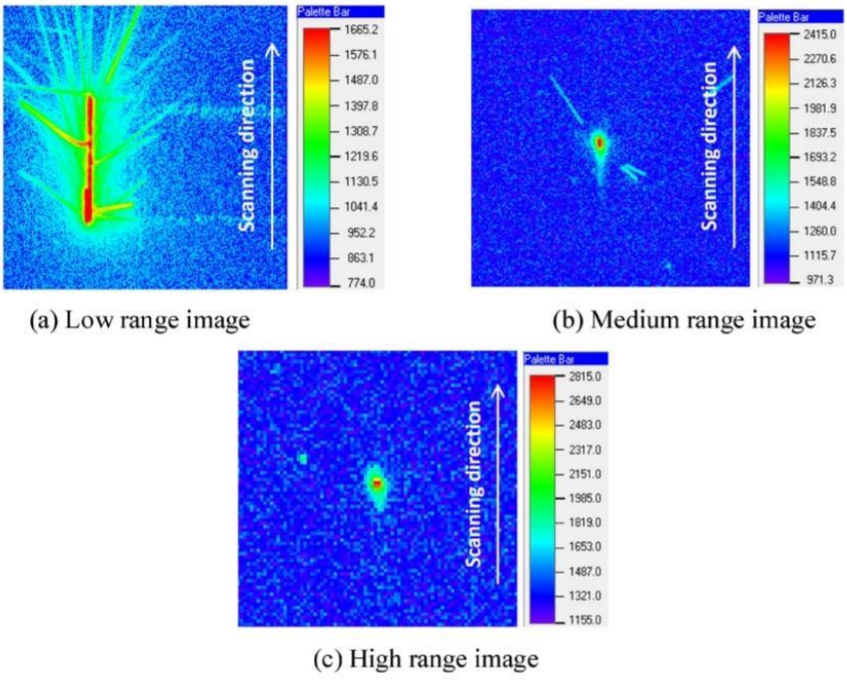

Figure.2.6 Typical thermal image (beam area) example of three temperature ranges at 400 mm/s speed for camera emissivity = 0.3 and transmission = 1.0.

2.9 Melt pool monitoring for laser beam melting of metals: assistance for material qualification for the stainless steel 1.4057

Tobias Kolb et al,(2018)

This project shows the results of a qualification procedure applying a coaxial melt pool monitoring system to determine suitable processing parameters for a material, which has not yet been processed. In this work, a stainless-steel material was exemplarily used to proof the feasibility. Furthermore, we are discussing the usability of this methodology for the material qualification in LBM-M in general.by this project we can show that for erain limits it is possible to check for reproducibilityof specimen manufactured with the same set of parameters using coaxial melt pool monitoring and also melt pool monitoring is usable for the detection of distortion.

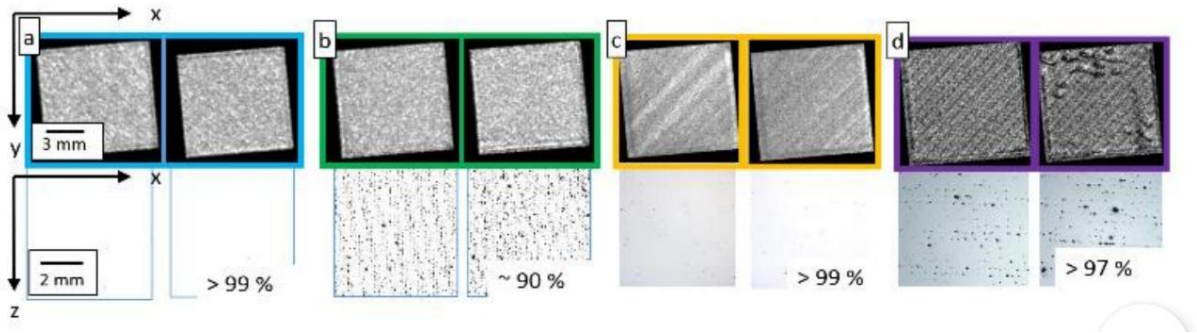

Figure.2.7.1 Camera melt pool images of different process gas zones with corresponding cross sections.

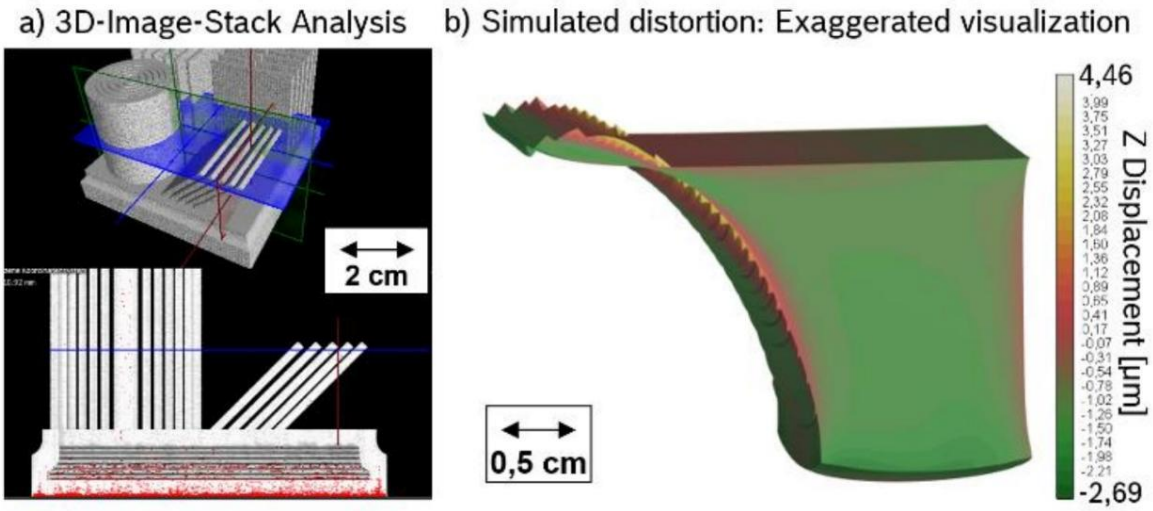

Figure.2.7.2 (a) Inspection of the melt pool image stack. Red accentuated regions represent larger melt pool areas. The bottom left image shows a concentration of such in the first layers; (b) simulation of z-displacement of overhang part (Amphyon, Additive Works GmbH) with exaggerated visualization. The model fails to predict the height of the displacement but helps understanding the process.

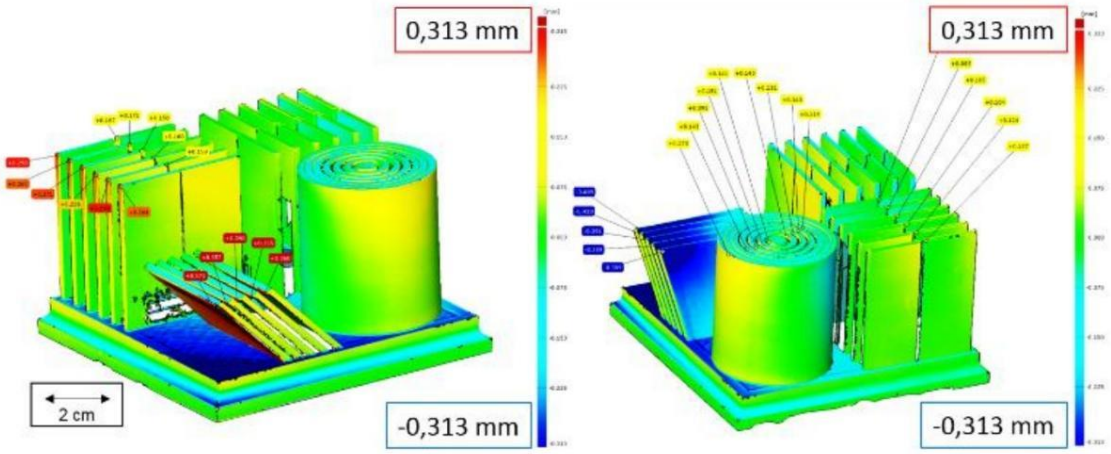

Figure.2.7.3 Two views onto a 3D-Scan for detection of geometrical deviations.

2.10 Experimental study and modelling of melt pool in laser powder bed fusion of thin walls

S.A.Egorov et al,(2020)

this project reviews the promising of manufacturing of lightweight cellular structures. Laser powder bed fusion (L-PBF) process parameters adopted for thin walls strongly differ from bulk material as melt pool formed on the top of thin wall is two dimensional. Ahigh speed CCD camera records a side view of the melt pool formed on the top of a thin metallic wall due to a laser beam scanning along the wall edge. The melt pool profile and the position of the keyhole are observed.

The results are compared with a two-dimensional model of coupled heat conduction and Marangoni convection in the laser-interaction zone. In the studied conditions, the best agreement between the experiment and the modelling implies that a keyhole is formed with the depth comparable with that of the melt pool. The length and depth of the calculated melt poolagree with the corresponding experimental parameters in assumption of formation of a deep keyhole.

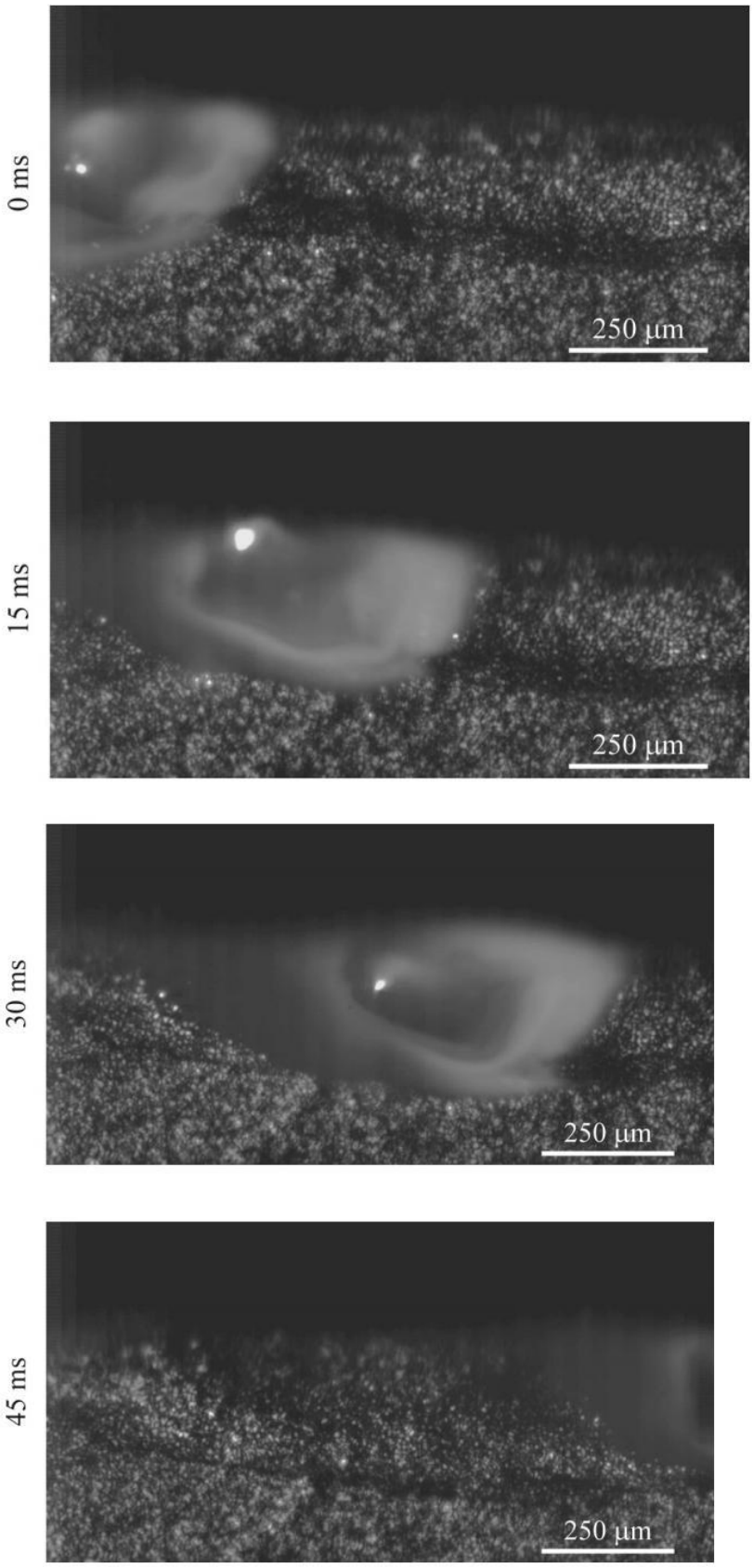

Figure.2.8 Profile views of the laser-interaction zone at the time instances indicated on the left.

2.11 Experimental analysis of spatter generation and melt-pool behaviour during the powder bed laser beam melting process.

V. Gunenthiram et al,(2017)

The experimental analysis of spatter formation was carried out on an instrumented SLM set-up allowing thequantification of spatter ejections and possible correlation with melt-pool behaviour.Fast camera analysisof powder beds indicated that droplet formation was mostly initiated in the powder-bed near the melt-poolinterface. On Al-12 Si alloys, such droplets were directly incorporated in the MP without being ejected upwardsas spatters like on 316L.

Lastly, it was shown that a complete suppression ofspatters was possible when using low volume energy densities combined with large spots to ensure sufficiently deep melt-pool penetrations.

2.12 Selective Laser Melting of 316L Stainless Steel: Physics of Melting Mode Transition and Its Influence on Microstructural and Mechanical Behaviour

AKASH AGGARWAL et al,(2018)

Selective laser melting (SLM), the most popular metal additive manufacturing (AM) process, is wellsuited for making complicated parts that are difficult to manufacture by conventional manufacturing techniques.

Melting is done by laser heat flux on the surface, so the melt pool formed is shallow and wider. However, in thekeyhole mode of melting, due to extremely high energy density, metal vaporizes and plasma is formed. The formationof a vapor cavity substantially increases the beam absorption enabling the laser to penetrate deeper, resultingin melt pools that are deeper and narrow. The conduction mode leads to high-quality stable melt pool formation with reduced spatter generation, whereas the keyhole mode of melting results in high penetration melts leading toenhanced productivity.

For focused laser beams, the keyhole mode of melting occurs where both the thermocapillary force and recoil pressure play a dominant role resulting in a narrow and deeper melt pool.

CHAPTER 3

COMSOL MULTIPHYSICS SOFTWARE

The Application Builder in the COMSOL Multiphysics® software makes it possible for simulation specialists to create easy-to-use simulation apps and deploy them within or outside of their organizations with COMSOL Server™ and COMSOL Compiler™. Thereby, high-fidelity physics simulation technology becomes accessible for everyone.

3.1.1 Streamline the Modeling Workflow

COMSOLMultiphysics enables you to simulate electromagnetics, structural mechanics, acoustics, fluid flow, heat transfer, and chemical phenomena in one environment, following one workflow. All simulation apps are created with the same tool, the Application Builder, independent of the type of physics involved.

3.1.2. Understand Product Behaviour

Using simulation apps, nonspecialists can run their own tests without needing to comprehend the complexities of the actual simulation. As a result, the whole organization can benefit from simulations, which in turn leads to an increased understanding of how their product will behave in the real world.

3.1.3.Collaborate Easily

Apps facilitate easy and seamless communication and the result is more (and better) collaboration between people with different functions inside or outside of an organization.

3.1.4. Provide Answers Quickly

A simulation app contains a limited amount of inputs, making it easy to set up the analysis. Experts might have fine-tuned a mesh, solver, or other conditions to solve a specific simulation fast. People with different backgrounds can run these simulations without having to ask the experts to do the job for them, or waiting for a full model to converge, helping them to get answers more quickly.

3.1.5. Free Up Resources

Simulation specialists can concentrate on developing new models and apps rather than having to run the same simulations over and over again. A developer can serve hundreds of users, and through the streamlined workflow the efficiency of the

organization is increased. In the end, companies adopting the creation, use, and distribution of simulation apps will be able to reduce errors early in the design phase and bring better products to market much faster.

3.1.6. Remove the Learning Curve

App users don’t need to understand the underlying technology of the simulation software to run an analysis with an app, as the inputs and outputs are restricted to what is pertinent to the analysis. By using simulation apps, anyone can test differentconfigurations and designs without needing to learn a new software tool.

3.2 STUDY

The Heat Transfer in Solids interface is used to model heat transfer by conduction, convection, and radiation. A Solid model is active by default on all domains. All functionality for including other domain types, such as a fluid domain, is also available.

The temperature equation defined in solid domains corresponds to the differential form of the Fourier's law that may contain additional contributions like heat sources.

Stationary, time-domain, and frequency-domain modeling are supported in all space dimensions.

The Time Dependent study is used when field variables change over time.

Examples: In electromagnetics, it is used to compute transient electromagnetic fields, including electromagnetic wave propagation in the time domain. In heat transfer, it is used to compute temperature changes over time. In solid mechanics, it is used to compute the time-varying deformation and motion of solids subject to transient loads. In acoustics, it is used to compute the time-varying propagation of pressure waves. In fluid flow, it is used to compute unsteady flow and pressure fields. In chemical species transport, it is used to compute chemical composition over time. In chemical reactions, it is used to compute the reaction kinetics and the chemical composition of a reacting system.

The Thermal Stress, Solid Multiphysics interface combines a Solid Mechanics interface with a Heat Transfer in Solids interface. The coupling occurs in domains, where the temperature from the Heat Transfer interface acts as a thermal load for the Solid Mechanics interface, causing thermal expansion. Optionally, effects from thermoelastic damping and inelastic dissipation can be used as heat sources in the heat transfer analysis.

CHAPTER 4

COMPUTATIONAL WORK:

4.1 Parameters used in SIMULATION:

Computational domain dimensions (μm)	7200 X 2400 X 600
Laser spot size (μm)	600
Pulse power (J)	1,2,3,4
Laser scan velocity (mm/s)	10,15,20,25
Ambient temperature (K)	293.15
Pulse width (ms)	0.5
Emissivity	0.7
Absorptivity	0.25
Convective heat transfer coefficient(w/m^2-k)	10

4.2 Properties of TITANIUM GRADE 9:

Composition and type	3%Al,2.5%V - Alpha annealed
Solidus temperature (K)	1977
Liquidus temperature (K)	1973
Melting point (K)	1973
Density (g/cc)	4.48
Hardness (BHN)	256
Ultimate tensile strength (Mpa)	620
Yield strength (Mpa)	500
Poissons ratio	0.3
Specific heat capacity (J/g-°C)	0.525
Thermal conductivity (W/m-k)	8.3 @temperature 23°C 11.8 @temperature 315°C
coefficient of thermal expansion (μm/°C)	9.86 @temperature 20°C-315°C

	9.97 @temperature 315℃-540℃
Shear modulus (Gpa)	44
Tensile modulus (Gpa)	100
Charpy impact (J)	86
Fatigue strength (Mpa)	170 @10^7 cycles
	280 @50000 cycles
	380 @40000 cycles

4.3 Selective governing equations and boundary conditions for Multiphysics model

Laser energy density, Ed(W/m^2)	$E_p/(Pw*(pi*0.25*D^2))$
Gaussian space, G_space	$\exp(-(((x-xr)^2)/(2*xd^2)))$
Laser heat source, pg(W/m^2)	A1*Ed*G_space
Convective heat loss	$h(T-T_\infty)$
Radiative heat loss	$\mathscr{E}\sigma(T^4-T_\infty^4)$

E_p-laser pulse power, Pw-pulse width of the laser, D-spot diameter of the laser beam, x-the domain in which we are working, xr-the reference point of the laser, xd-standard deviation, Ed-laser energy density, $\mathscr{E}$-emissivity, h-convective heat transfer coefficient, T-temperature of the block, σ-stefan Boltzmann constant, T_∞-temperature of the surroundings.

4.4 Simulation

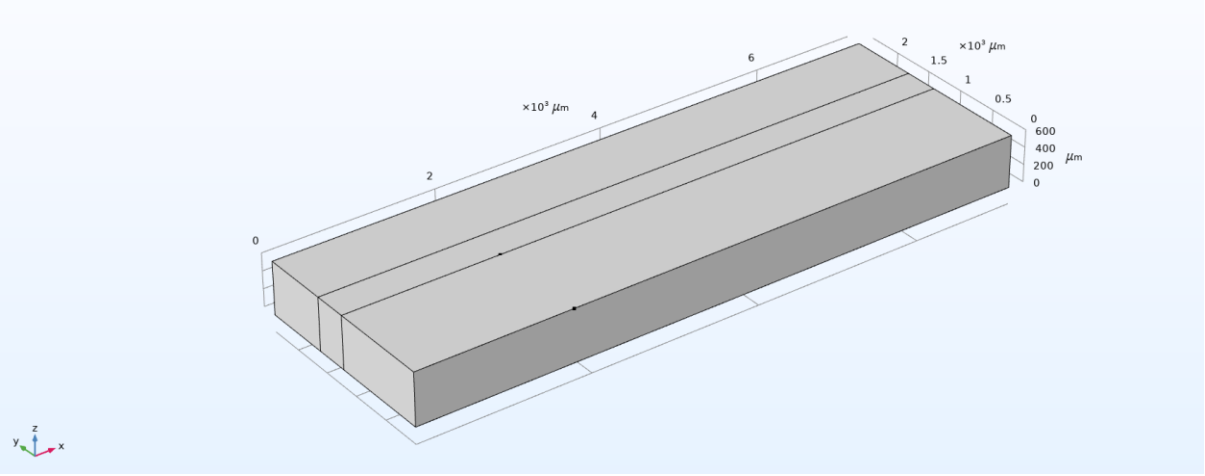

Figure.4.1 Schematic of the computational domain (all dimensions are in µm)

In this domain the laser beam ismoving continuously along the principle longitudinal axis (X-axis)with predefined scanning speed (Vin) and pulse rate or pulses persecond (f) to complete each laser track.

A computational model was designed and developed on the basis of aMultiphysics approach on commerciallyavailable COMSOLTM finite-element platform to precisely mimic the moving laser source for meltpool analysis of titanium grade 9. To achieve higher modelling accuracy, the present multiphysics (Heat transfer in solids and solid mechanics)computationalmodel incorporated temperature-dependent material properties of Titanium grade 9 available in the open literaturethe phase change effects due to temperature along with body force.

The other modelling assumptions are: (i) laser beam profile is in Gaussian distribution (TEM00 mode), (ii) mate- rial is isotropic and opaque, (iii)evaporated/ablated material istransparent and does not interfere with the incident laser beam, and (iv) multiple reflections of laser radiation within the crater are neglected.

The selected key governing equations and important boundary conditions for heat flux, natural convection cooling and radiation, volume force are summarised in the table.The present computational model used the temperature dependent materials properties to accurately simulate phase change phenomena in this analysis.However, it is worth mentioning that although typically the emissivity (ε) varies significantly with temperature, in the present case a constant value of 0.7 was considered due to the paucity of availability of the temperature dependent emissivity of titanium in the open literature.

The occurrence of multiple physical phenomena in such short duration makes it, if not impossible, very difficult either to conduct in situ experimental measurements

or design a computational model for obtaining temperature dependent emissivity values. This is further complicated with the high temperatures associated with such physical changes in titanium.

It is pointed out here that the governing Eq.is a function of temperature. The evolution of temperature within the laser beam material interaction region depends on laser beam pulse energy (Ep), pulse width (Pw), pulse rate or pulses per second (f), and laser beam scanning speed (Vin). In light of this, the computational model developed in the present work inherently associated with the moving laser beam. As the computational model was developed with a quasi-stationary laser beamapproach in which the development (evolution) of temperature and associated effects were considered with a finite laser residence time (or pulse width) that in turn is dictated by the laser scanning speed.

On the topboundary, convective and radiation heat losses occur and the

net heat flow is equal to the balance of incident beam heat energy and convective and radiation heat losses.

4.5 Meshing

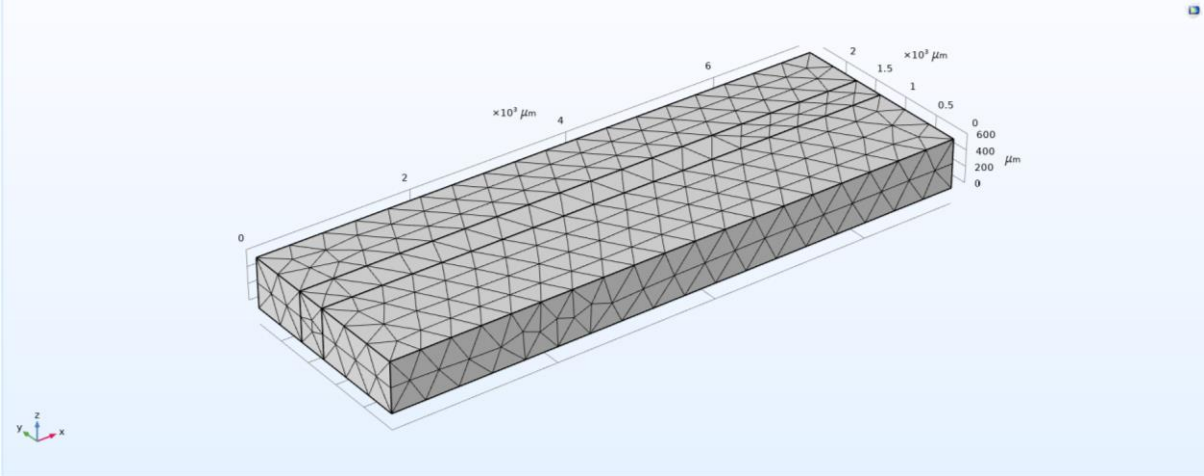

Figure.4.2 Finer mesh used for the domain

The mesh that we choose for our COMSOL Multiphysics simulation strongly affects our modeling requirements. In fact, meshing is one of the most memory-intensive steps when it comes to setting up and solving a finite element problem.

Identifying the mesh best-suited for your particular model often involves choosing the correct element types and sizes. In COMSOL Multiphysics, meshing utilizes four different element types: tetrahedra (tets), hexahedra (bricks), triangular prisms (prisms), and pyramids. There are also nine preset element size settings, which range from Extremely fine to Extremely coarse.

Meshing, like many of the tools available in COMSOL Multiphysics, is customizable and interactive. In just a few steps, you can easily mesh individual faces or domains. Further, the default physics-controlled meshing sequences create meshes that consist of different element types and size features, which you can use as a starting point to add, move, disable, and delete meshing operations. Each meshing operation is built in the order it appears in the meshing sequence to produce the final mesh. Customizing the meshing sequence can help reduce memory requirements by controlling the number, type, and quality of elements, thereby creating an efficient and accurate simulation.

It is also possible to use the default Physics-controlled mesh settings. Depending upon the physics involved in the model, the software will adjust the mesh based upon the geometry, and possibly also the applied domain and boundary conditions within the physics as well as the materials properties.To gain confidence in the accuracy of our model, we must re-solve the model on progressively finer meshes and compare results. In the limit of mesh refinement, well-posed problems will be convergent.

CHAPTER 5

RESULTS AND DISCUSSONS

5.1Temperature distribution in the computational domain for gaussian power corresponding to pulse power 1J and scanning speed as 25mm/s.

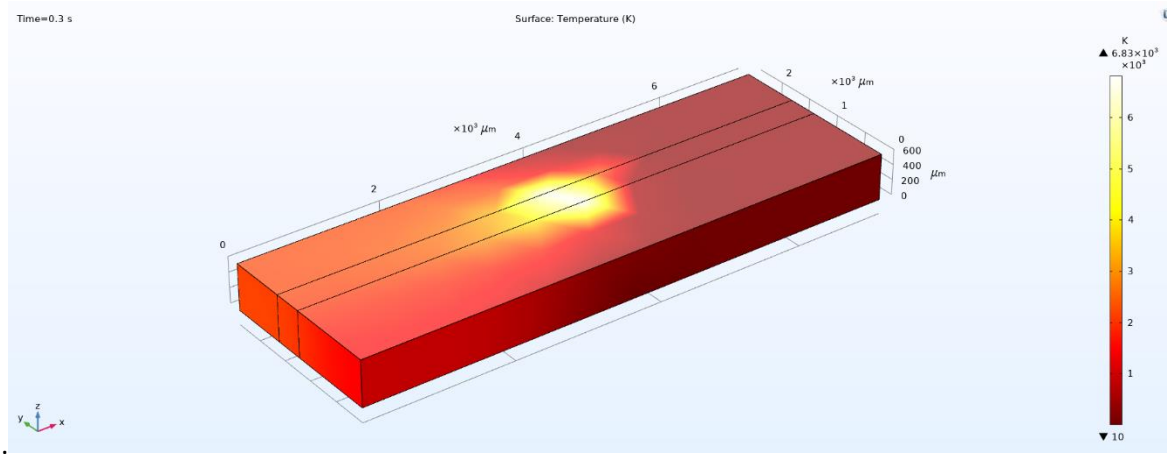

Figure.5.1.1 Time=0.3s, pulse power=1J, v=25mm/s

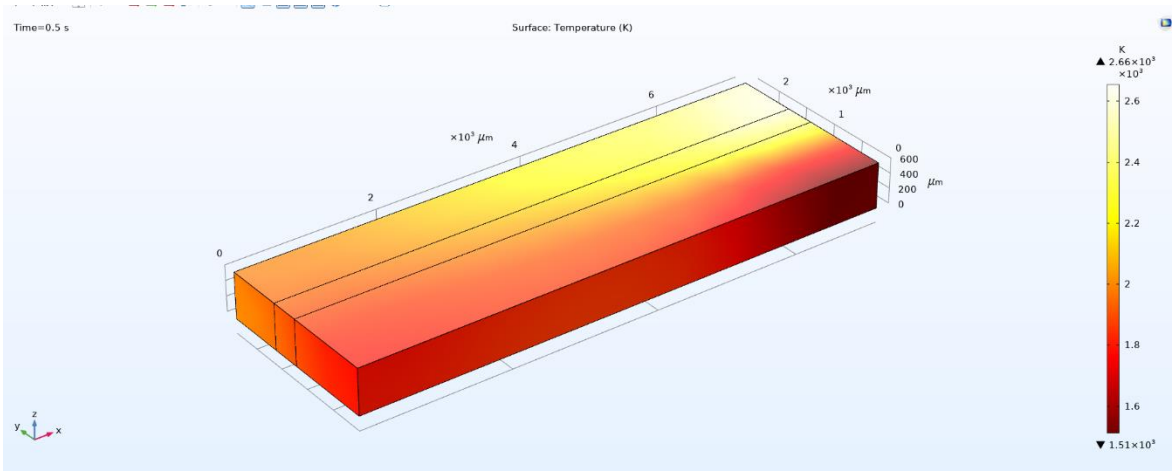

Figure.5.1.2 Time=0.5s, pulse power=1J, v=20mm/s

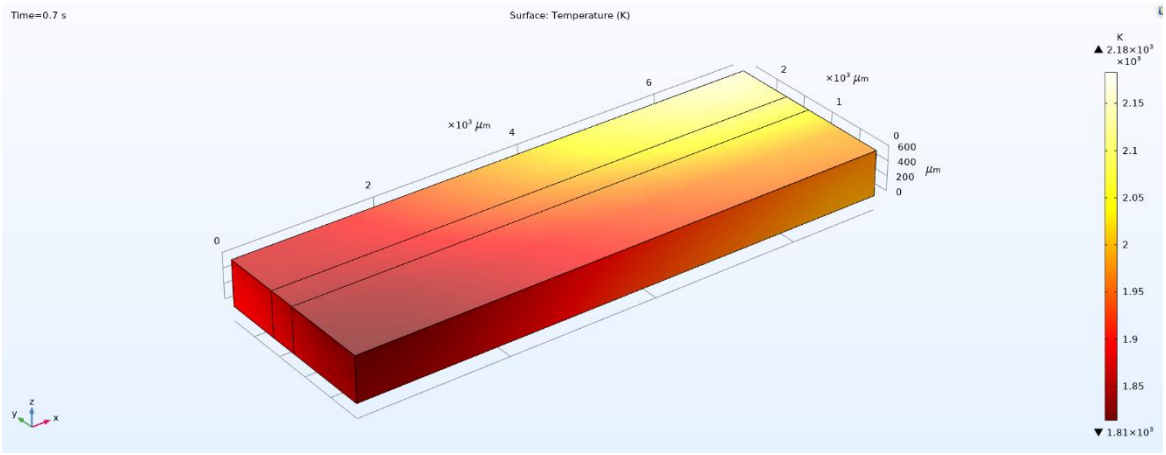

Figure.5.1.3Time=0.7s, pulse power=1J, v=25mm/s

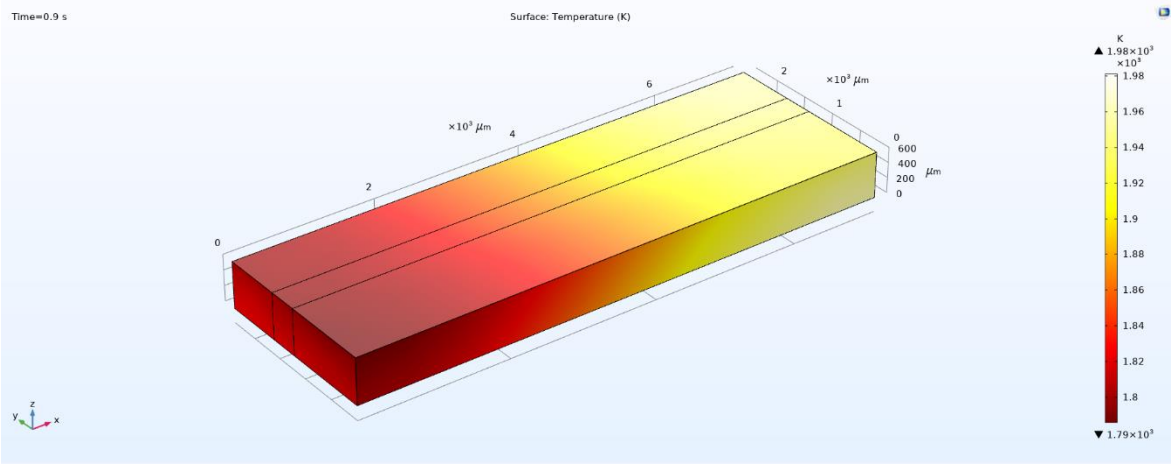

Figure.5.1.4Time=0.9s, pulse power=1J, v=25mm/s

From the above simulation results it is observed that the temperature distribution depends on three parameters

- Input energy (Ep)
- Scanning speed (V)
- Diameter of Laser beam (D)

We noticed that temperature decreases with respect to time. When the input energy is 1J and scanning speed as 25mm/s the maximum temperature is 6830k and the minimum temperature observed is 1980k.

5.2 Thermal Stress distribution in the computational domain for gaussian power corresponding to pulse power 1J and scanning speed as 25mm/s.

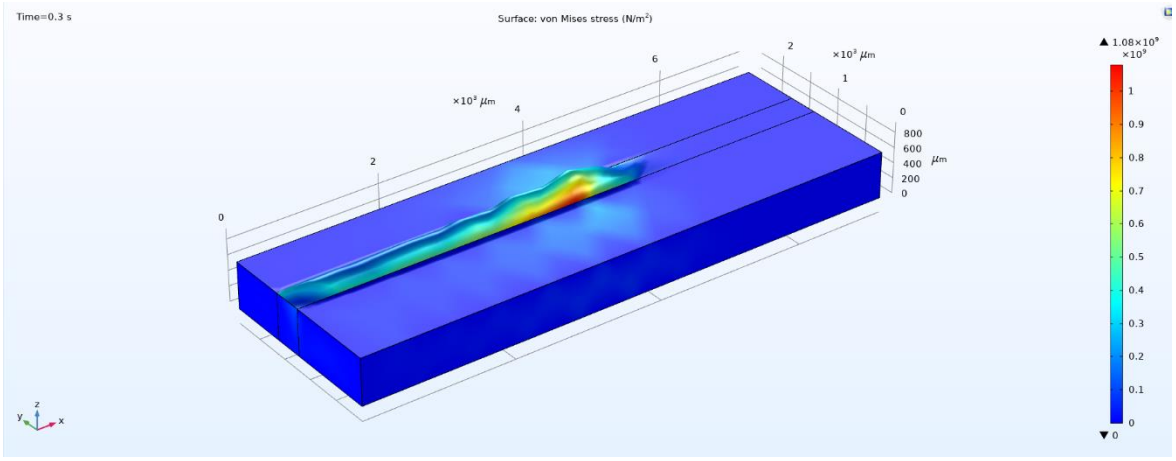

Figure 5.2.1 Time=0.3s, pulse power=1J, v=25mm/s

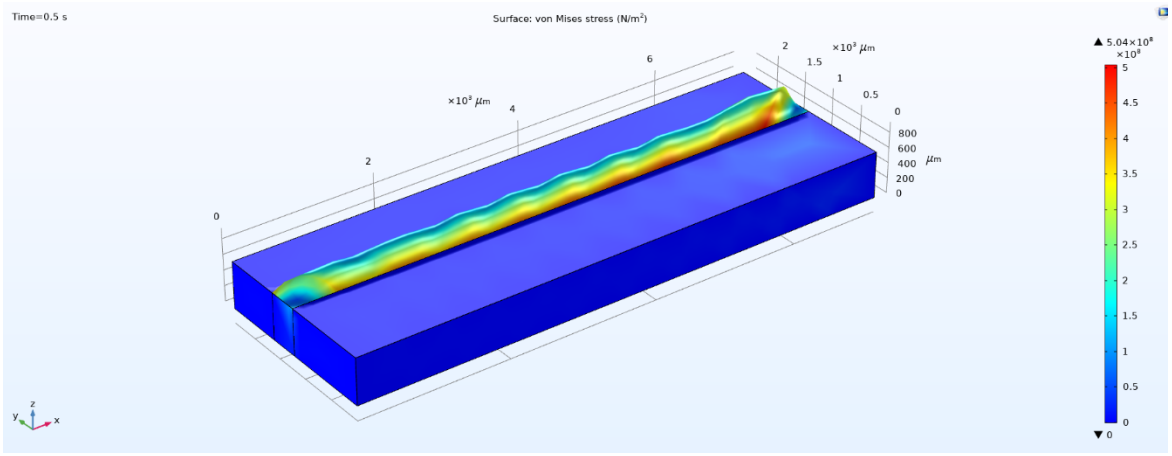

Figure 5.2.2 Time=0.5s, pulse power=1J, v=25mm/s

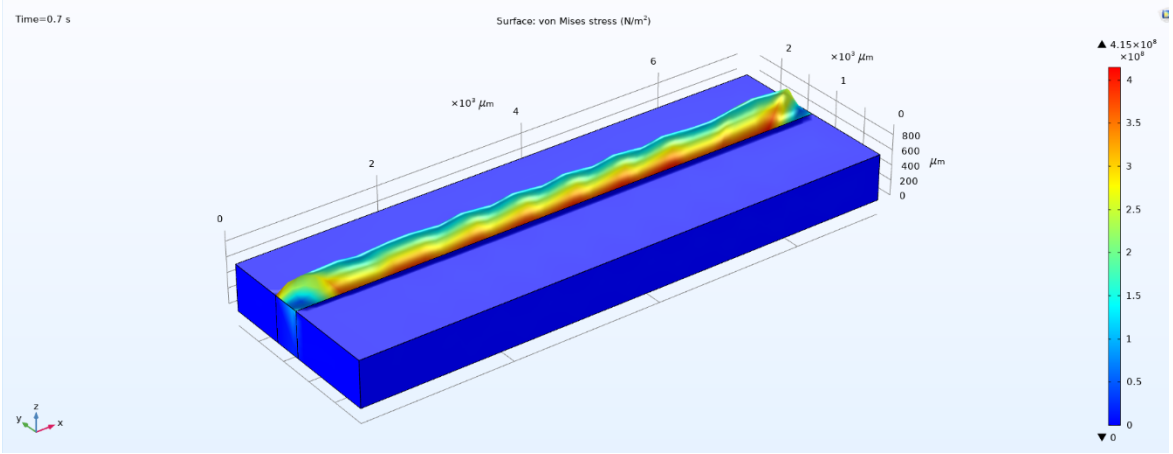

Figure 5.2.3 Time=0.7s, pulse power=1J, v=25mm/s

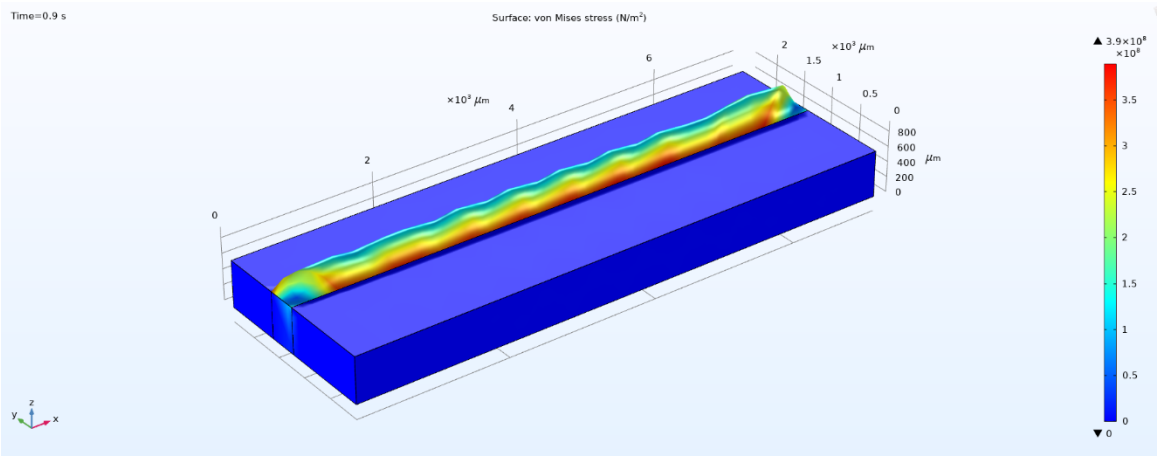

Figure 5.2.4 Time=0.9s, pulse power=1J, v=25mm/s

Laser beam contains very high temperature, so that this temperature distributes to our body. Stress is the external forces acting per unit area. The force can be of any form. When the applied force is in the form of temperature the resultant force is called Thermal stress. It is observed that when an object expands or contracts due to a change in temperature. Thus, we can define thermal stress.

Von Misses is credited with coming up with what is arguably the most accepted yield criterion (way of resolving these stresses). He designed an equation that takes in each shear and principal stress value, and in turnspits out a single "von Misses stress value", which can be compared to a yield strength of the material. If the value is greater than the yield strength, the part is failing according to his criteria. If it is less, then the part is said to be within the yield criteria and is not failing (for yield failure only).

Thermal stress deceases with respect to time as temperature also decreases with respect to time. It is observed that the maximum thermal stress is 1.08Gpa and the minimum thermal stress is 0.39Gpa.

5.3 Principal stress tensor

Principal stresses are those stresses which are acting on the principal planes. The plane carrying the maximum normal stress is called the major principal plane and stress acting on it is maximum principal stress. **Principal stress tensor** which is also called **Cauchy stress tensor** consists of nine components σ_{ij}that completely define the state of stress at a point inside a material in the deformed state, placement or configuration.

The tensor relates a unit-length direction vector n to the traction vector T(n) across an imaginary surface perpendicular to n.

$$T^{(n)}=n.\sigma \quad \text{or} \quad T_j^{(n)}=\sigma_{ij}.n_i \qquad \text{----------(5.1)}$$

Stress tensor is given by

$$\sigma = \begin{pmatrix} \sigma_{xx} & \sigma_{xy} & \sigma_{xz} \\ \sigma_{yx} & \sigma_{yy} & \sigma_{yz} \\ \sigma_{zx} & \sigma_{zy} & \sigma_{zz} \end{pmatrix} \qquad \text{----------(9.2)}$$

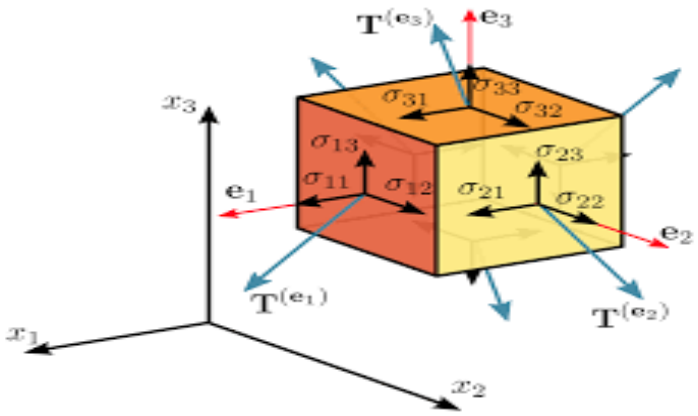

Figure.5.3.1 Schematic of principal stresses and principal strains

In this simulation we obtained 9 stress components along x,y and z directions respectively. The below figures are the results of simulation and its distribution throughout the component when the pulse power is 1J and scanning speed with 25mm/s.

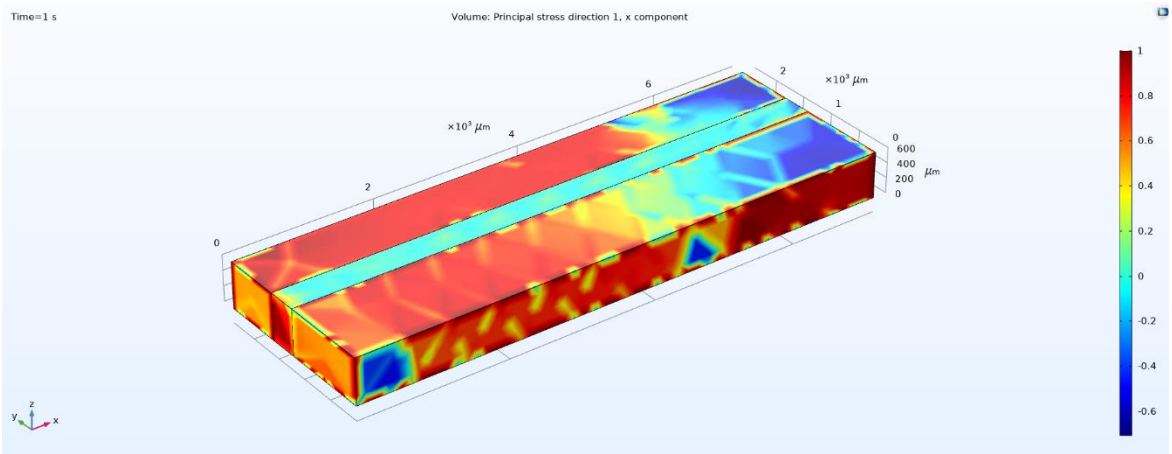

Figure.5.3.2 Schematic of principal stress distribution 1, X component

Principal stress 1, X component means the positive normal stress in YZ plane along X direction. The above picture is the representation of principal stress distribution throughout the component and it is observed that the maximum effected region is subjected totensile stress.

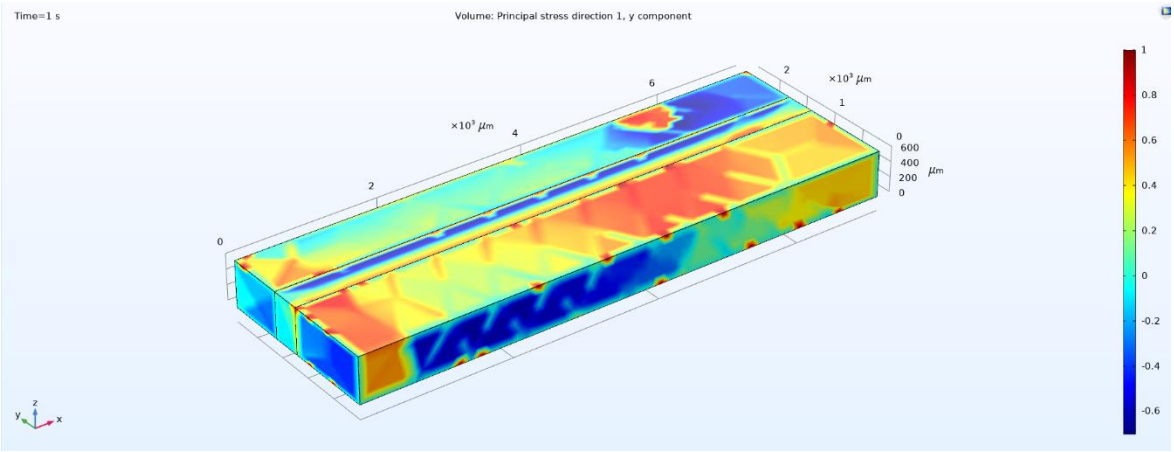

Figure.5.3.3 Schematic of principal stress distribution 1, Y component

Principal stress 1, Y component means the negative normal stress in YZ plane along Y direction. The above picture is the representation of principal stressdistribution throughout the component and it is observed that the maximum effected region is in compressive in nature.

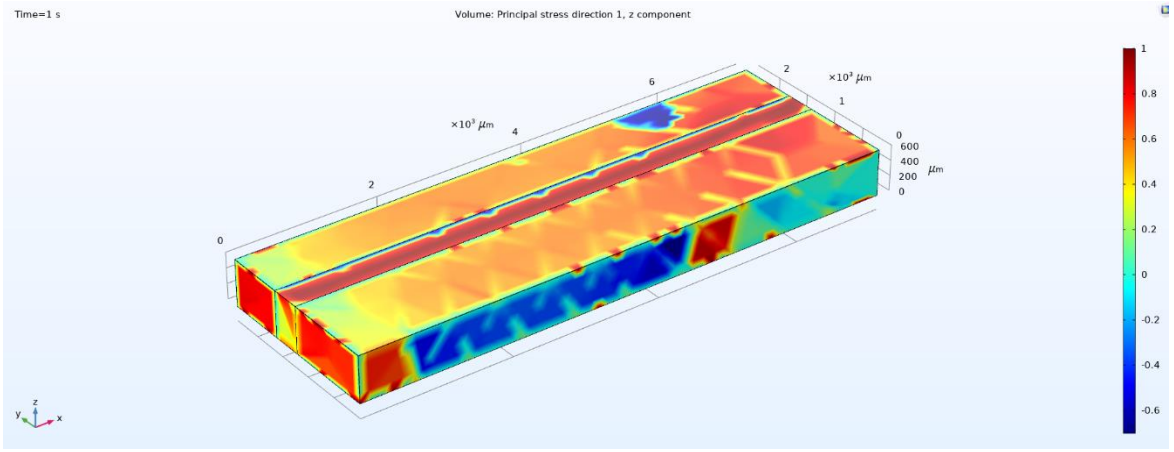

Figure.5.3.4 Schematic of principal stress distribution 1, Zcomponent

Principal stress 1, Z component means the negative normal stress in YZ plane along Z direction. The above picture is the representation ofprincipal stressdistribution throughout the component and it is observed that the maximum effected region is in tensile in nature with about 70% of the maximum stress.

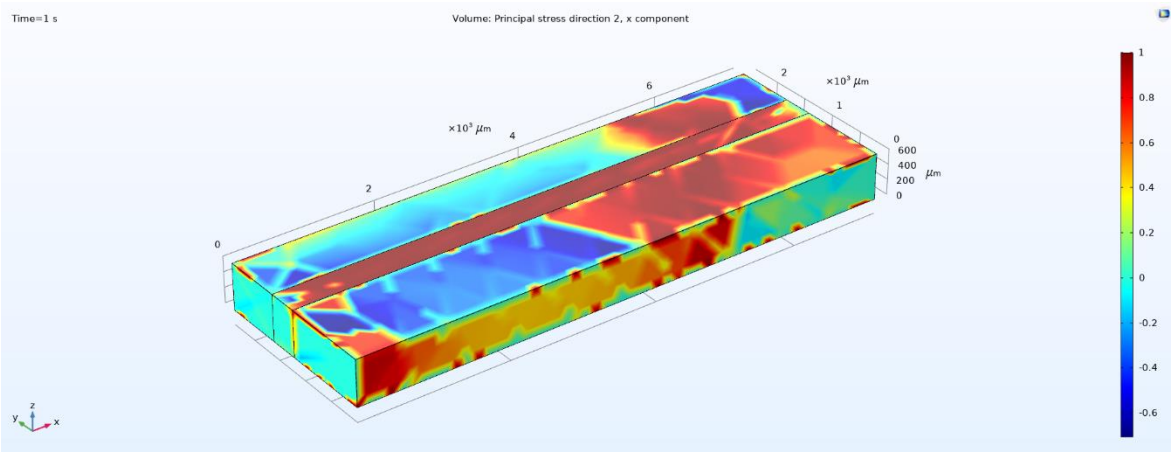

Figure.5.3.5 Schematic of principal stress distribution 2, X component

Principal stress2, X component means the negative normal stress in XZ plane along X direction. The above picture is the representation of principal stressdistribution throughout the component and it is observed that the maximum effected region is in compressive in nature with about 50% of the maximum stress.

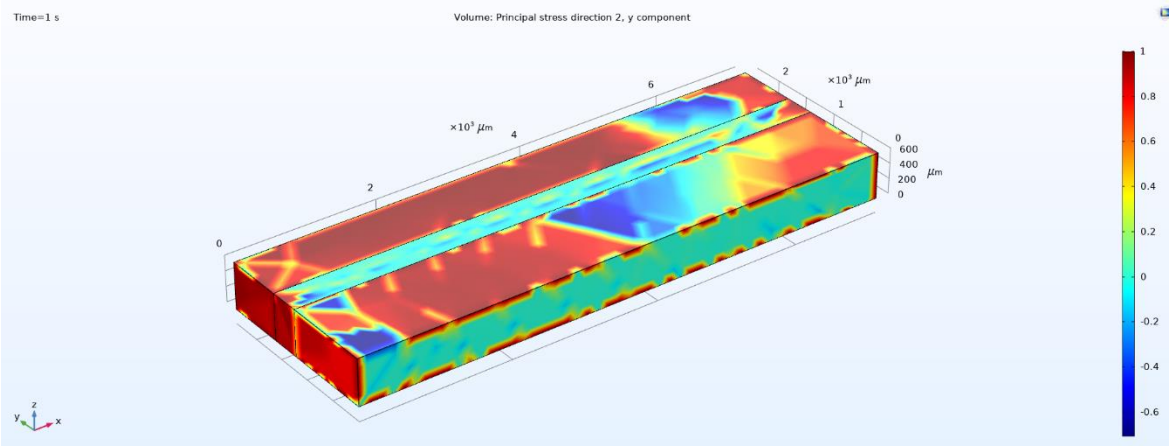

Figur5.3.6 Schematic of principal stress distribution 2, Ycomponent

Principal stress 2, Y component means the negative normal stress in XZ plane along Y direction. The above picture is the representation ofprincipal stressdistribution throughout the component and it is observed that the maximum effected region is in tensile in nature.

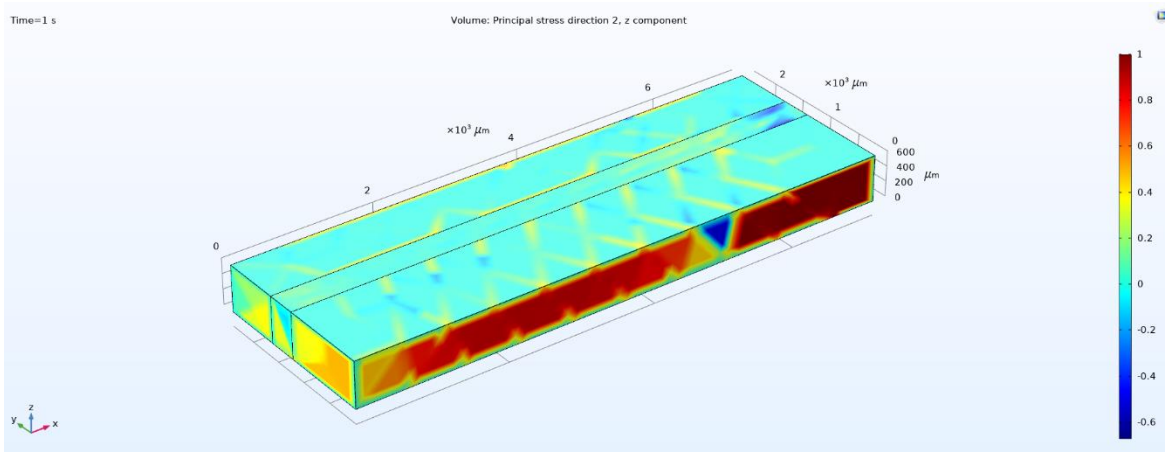

Figure.5.3.7 Schematic of principal stress distribution 2, Z component

Principal stress 2, Z component means the negative normal stress in XZ plane along Z direction. The above picture is the representation of principal stress distribution throughout the component and it is observed that the component is totally subjected to compressive stress.

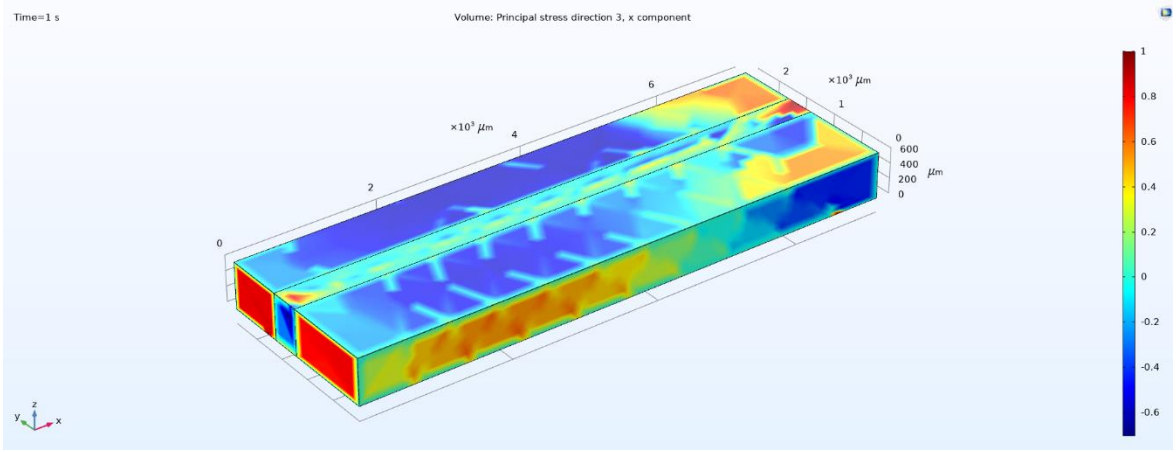

Figure.5.3.8 Schematic of principal stress distribution 3, X component

Principal stress3, X component means the negative normal stress in XY plane along X direction. The above picture is the representation of principal stressdistribution throughout the component and it is observed that the maximum effected region is in compressive in nature with about 50% of the maximum stress.

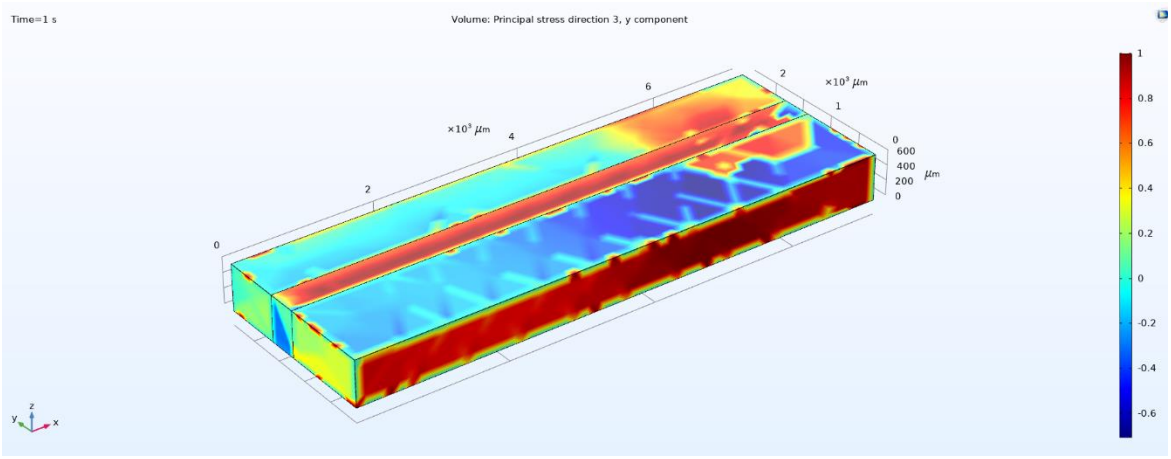

Figure.5.3.9 Schematic of principal stress distribution 3,Ycomponent

Principal stress3, Y component means the negative normal stress in XY plane along Y direction. The above picture is the representation of principal stress distribution throughout the component and it is observed that the maximum effected region is in compressive in nature with about 50% of the maximum stress.

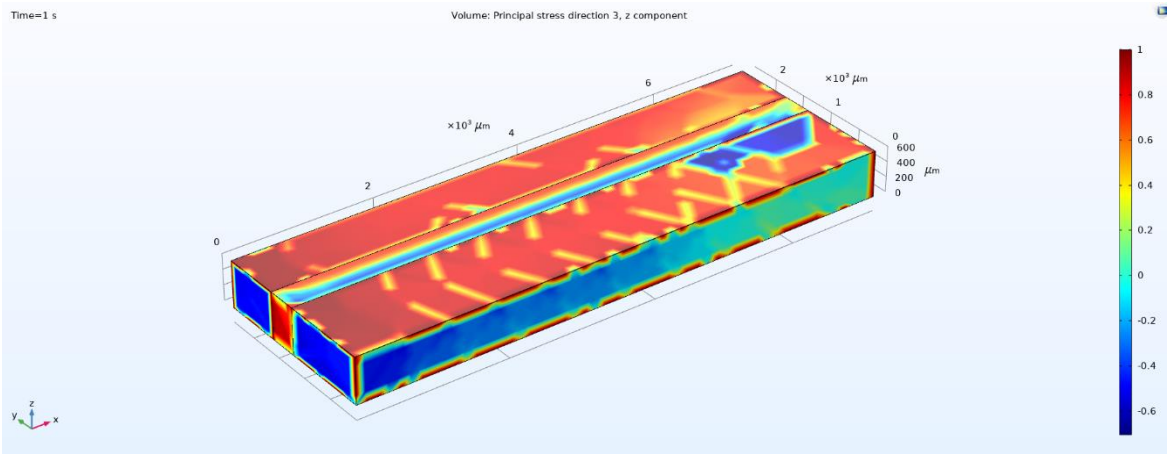

Figure.5.3.10 Schematic of principal stress distribution 3, Z component

Principal stress 3, Z component means the negative normal stress in XY plane along Z direction. The above picture is the representation of principal stress distribution throughout the component and it is observed that the maximum effected region is in tensile in nature.

5.4 Temperature gradient

A temperature gradient is a physical quantity that describes in which direction and at what rate the temperature changes the most rapidly around a particular location. The temperature gradient is a dimensional quantity expressed in units of degrees (on a particular temperature scale) per unit length. The SI unit is kelvin per meter (K/m).

Assuming that the temperature T is an intensive quantity, i.e., a single-valued, continuous and differentiable function of three-dimensional space (often called a scalar field), i.e., that

$$T = T[X, Y, Z] \qquad \text{----------(5.3)}$$

where x, y and z are the coordinates of the location of interest, then the temperature gradient is the vector quantity defined as

$$\nabla T = [\partial T/\partial X\ ,\ \partial T/\partial Y,\ \partial T/\partial Z\ ] \qquad \text{----------(5.4)}$$

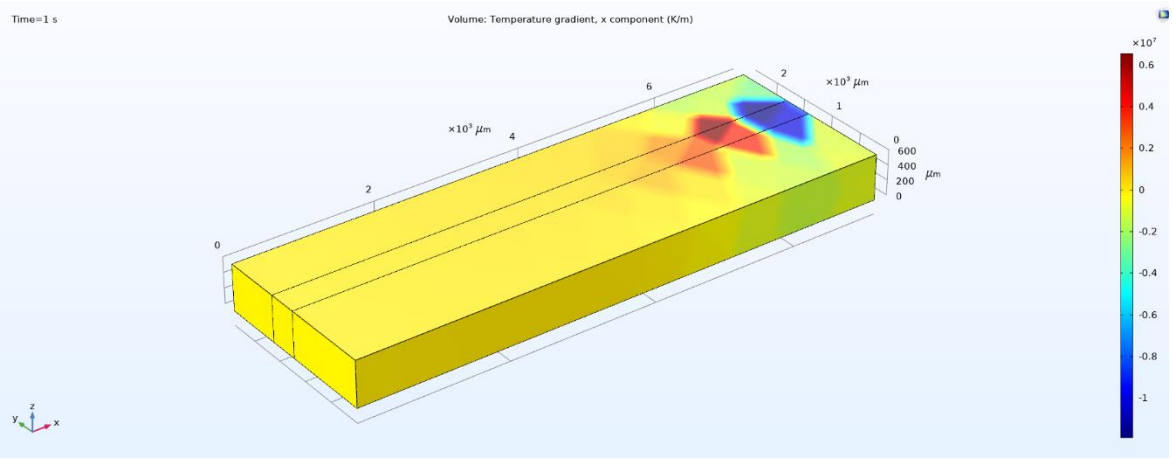

Figure.5.4.1Schematic of Temperature gradient, X component

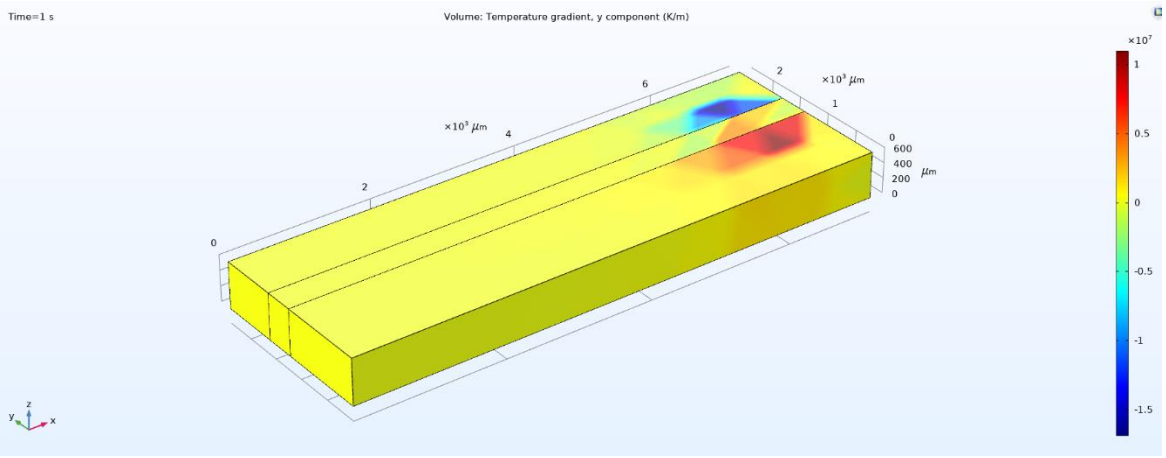

Figure.5.4.2Schematic of Temperature gradient, X component

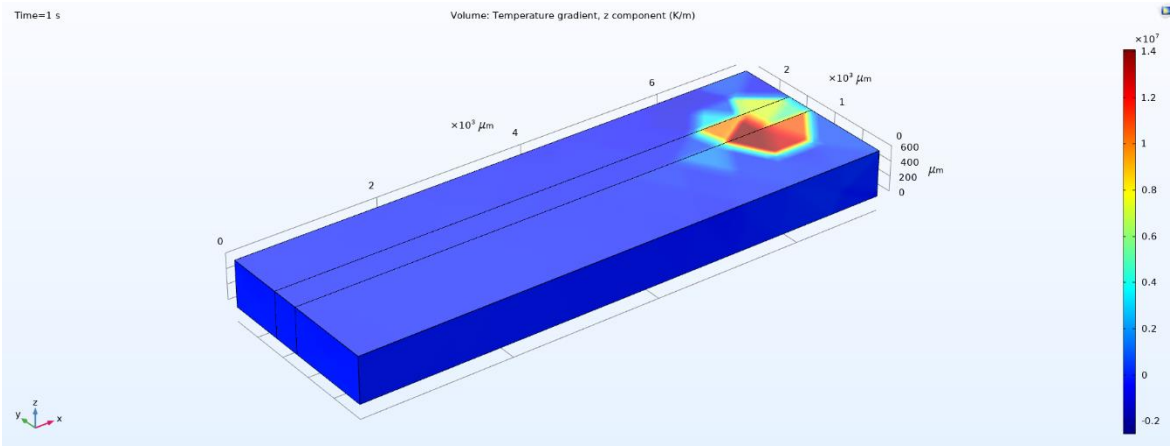

Figure.5.4.3Schematic of Temperature gradient, X component

The above images showed the Temperature gradient in 3 different directions namely X, Y and Z respectively when the pulse power of Laser is 1J and the corresponding scanning speed is 25 mm/s. Temperature gradient is positive along X and Y directions whereas it is negative along Z axis.

5.5 Volumetric strain

Volumetric strain of a deformed body is defined as the ratio of the change in volume of the body to the deformation to its original volume. If V is the original volum and dV the change in volume occurred due to the deformation, the volumetric strain ev induced is given by.

$$e_v = [\, dV/V] \qquad \text{----------(5.5)}$$

Where e_v is the volumetric strain, dV is the change in volume of the body and V is the total volume of the body. The below figure is showing the Volumetric strain and it is observed that the distribution of strain is less.

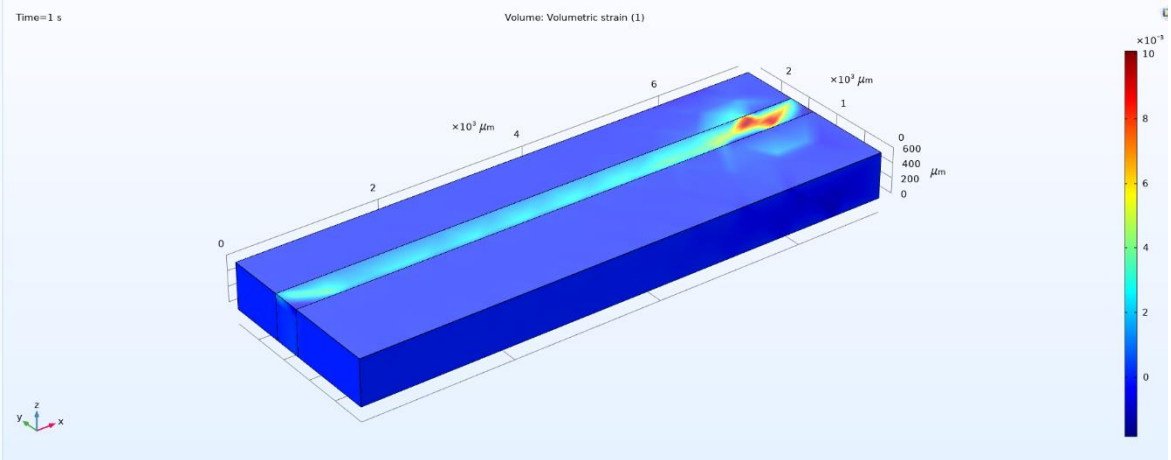

Figure.5.5 Schematic of Volumetric strain

5.6 Tabulation of the Results

s.no	Pulse power (E_p)	1J		2J		3J		4J	
	Time(s)	T (K)	σ(Gpa)	T (K)	σ(Gpa)	T (K)	σ(Gpa)	T (K)	σ(Gpa)
1	0.3	295	0.000245	297	0.000383	299	0.000574	301	0.000765
2	0.5	9230	1.4	12800	1.95	15000	2.26	16600	2.5
3	0.7	8140	1.34	11400	1.83	13700	2.12	15400	2.33
4	0.9	8550	1.34	11800	1.79	13800	2.06	15300	2.28

Table 5.1: Computational results for the scanning speed V=10 mm/s

s.no	Pulse power (E_p)	1J		2J		3J		4J	
	Time(s)	T (K)	σ(Gpa)	T (K)	σ(Gpa)	T (K)	σ(Gpa)	T (K)	σ(Gpa)
1	0.3	9130	1.21	1300	1.73	15300	2.03	17000	2.26
2	0.5	7890	1.25	11700	1.8	14100	2.12	15800	2.35
3	0.7	8160	1.18	11700	1.61	13900	1.88	15600	2.08
4	0.9	2920	0.554	3370	0.647	3550	0.682	46600	6.98

Table 5.2: Computational results for the scanning speed V=15 mm/s

s.no	Pulse power (E_p)	1J		2J		3J		4J	
	Time(s)	T (K)	σ(Gpa)	T (K)	σ(Gpa)	T (K)	σ(Gpa)	T (K)	σ(Gpa)
1	0.3	8030	1.15	11500	1.75	13500	2.12	14900	2.38
2	0.5	8620	1.01	12700	1.52	15000	1.82	16700	2.03
3	0.7	2680	0.492	3270	0.615	3490	0.66	3630	0.686
4	0.9	2250	0.442	2630	0.53	2770	0.557	2830	0.571

Table 5.3: Computational results for the scanning speed V= 20 mm/s

s.no	Pulse power (E_p)	1J		2J		3J		4J	
	Time(s)	T (K)	σ(Gpa)	T (K)	σ(Gpa)	T (K)	σ(Gpa)	T (K)	σ(Gpa)
1	0.3	6830	1.08	11400	1.68	13600	2.03	15500	2.27
2	0.5	2660	0.504	3530	0.67	3890	0.746	4150	0.789
3	0.7	2180	0.415	2710	0.534	2890	0.574	2990	0.594
4	0.9	1980	0.39	2380	0.483	2510	0.511	2570	0.525

Table 5.4: Computational results for the scanning speed V= 25 mm/s

5.7 Graphical Representation of the Simulation results

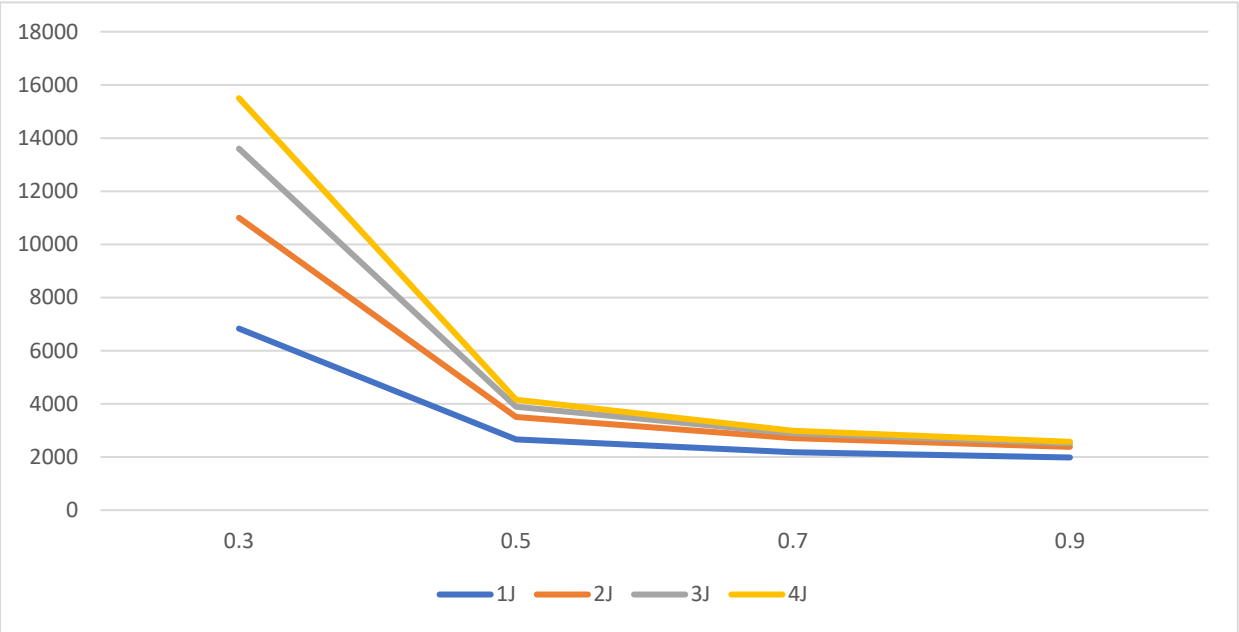

Figure 5.6: Temperature distribution(k) vs time(s) at v=25mm/s

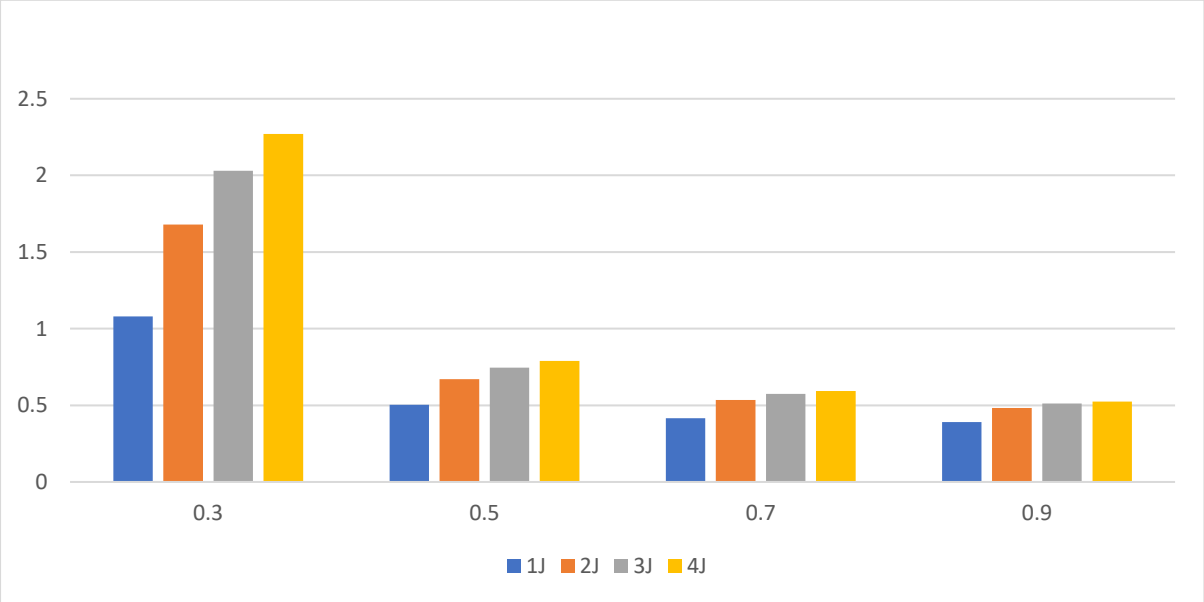

Figure 5.7: Thermal stress (Gpa) vs time(s) at v =25 mm/s

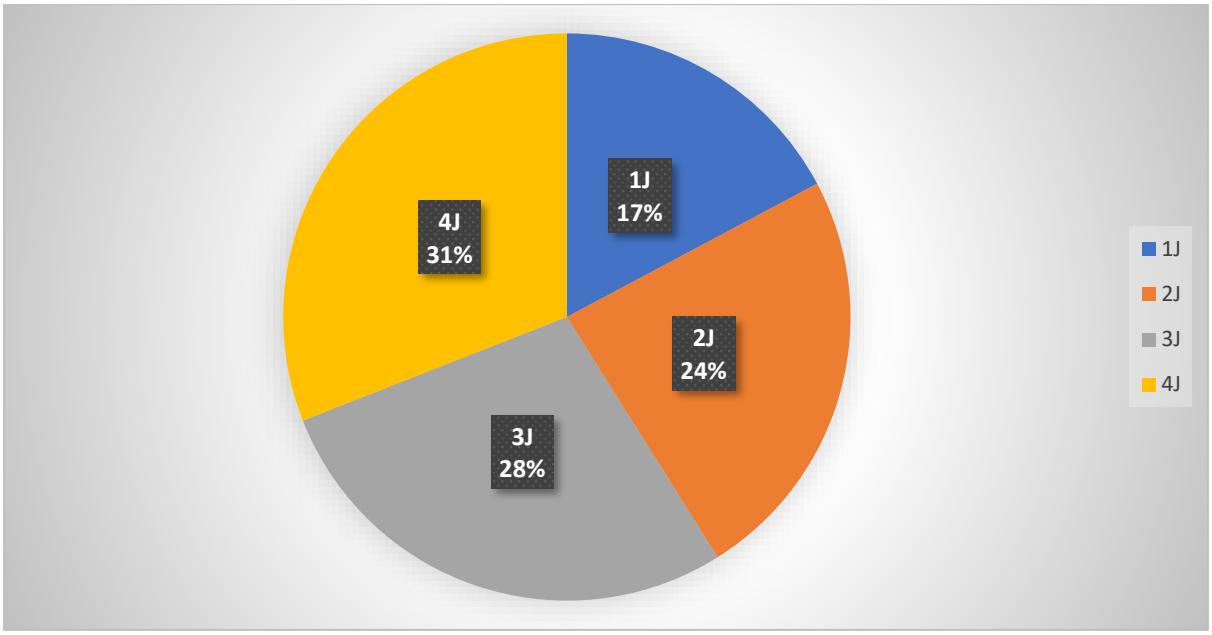

Figure 5.8: Maximum temperature (k) at v=10 mm/s

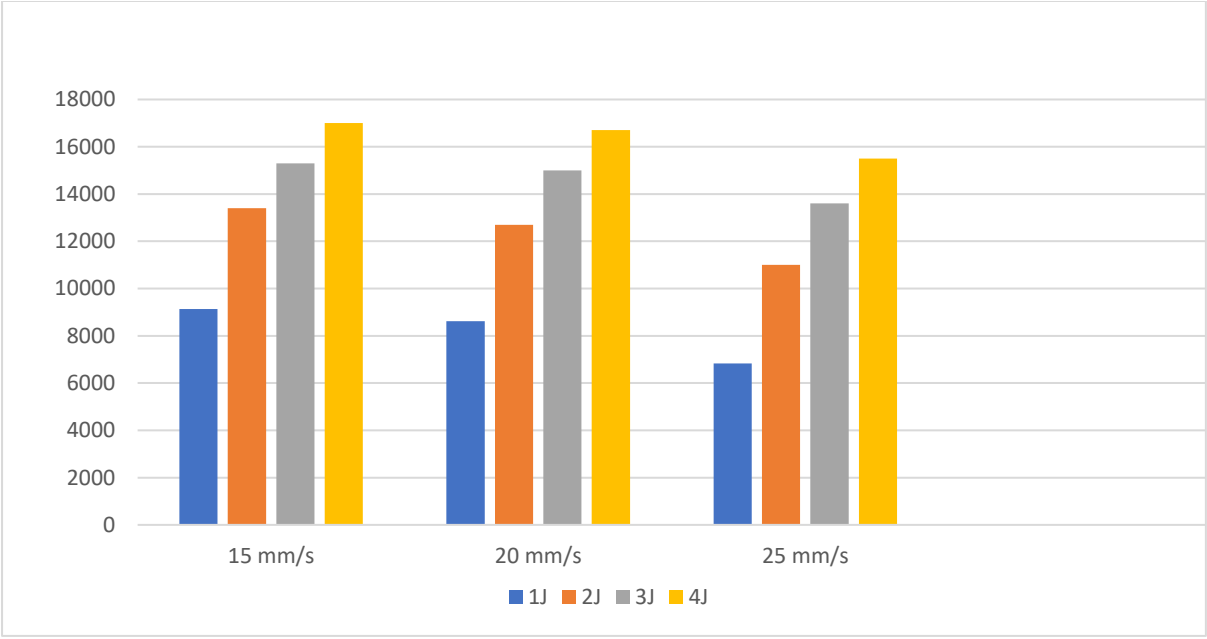

Figure 5.9: Maximum Temperature vs time(s) at Ep= 1J for scanning speeds 15,20,25mm/s

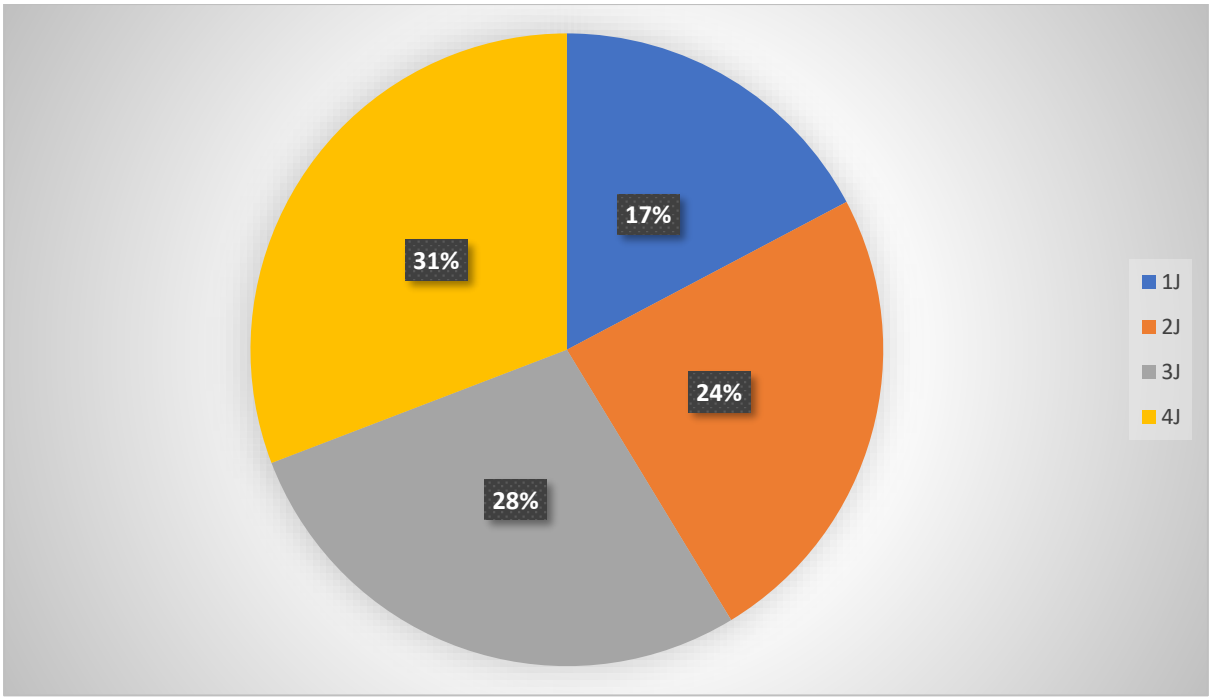

Figure 5.10: Maximum thermal stress (Gpa) at v=10 mm/s

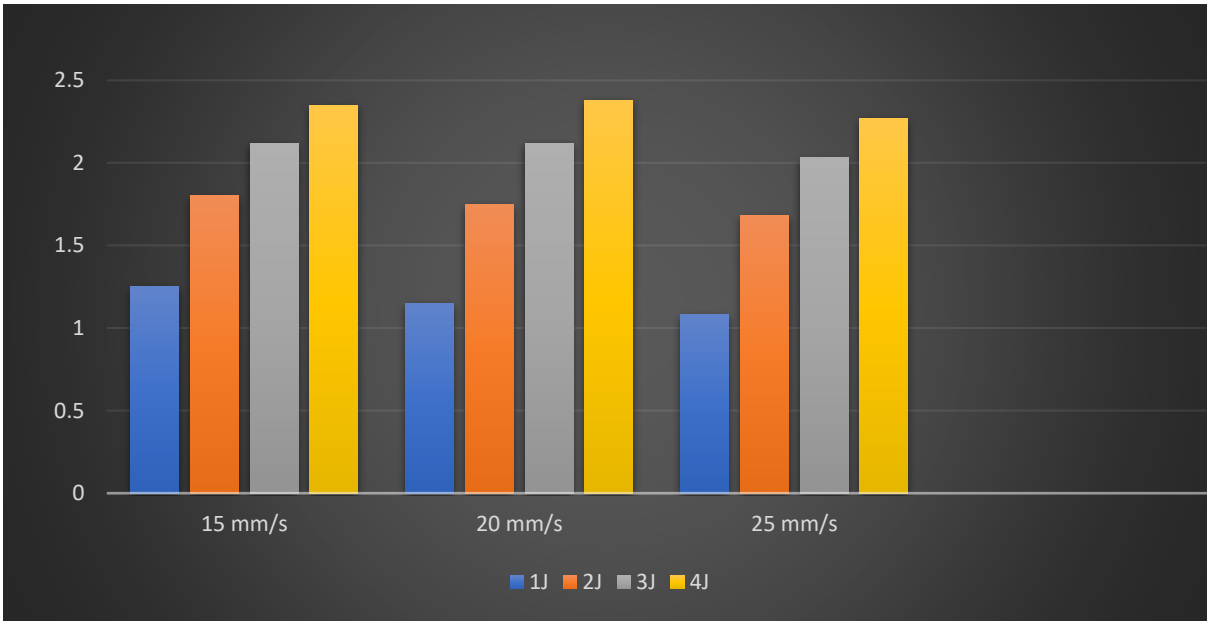

Figure 5.11: maximum stress (Gpa) vs time (s) for scanning speeds 15,20 and 25mm/s at Ep=1J

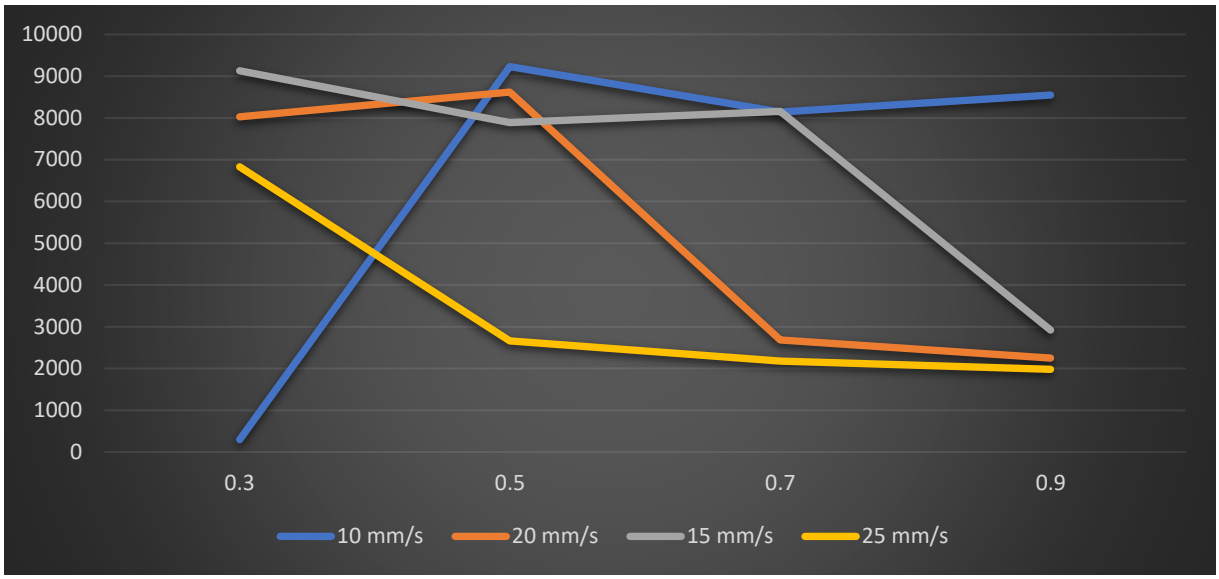

Figure 5.12: Temperature (k) vs time (s) at all scanning speeds for Ep=1J

5.8 1- D Plot graphs

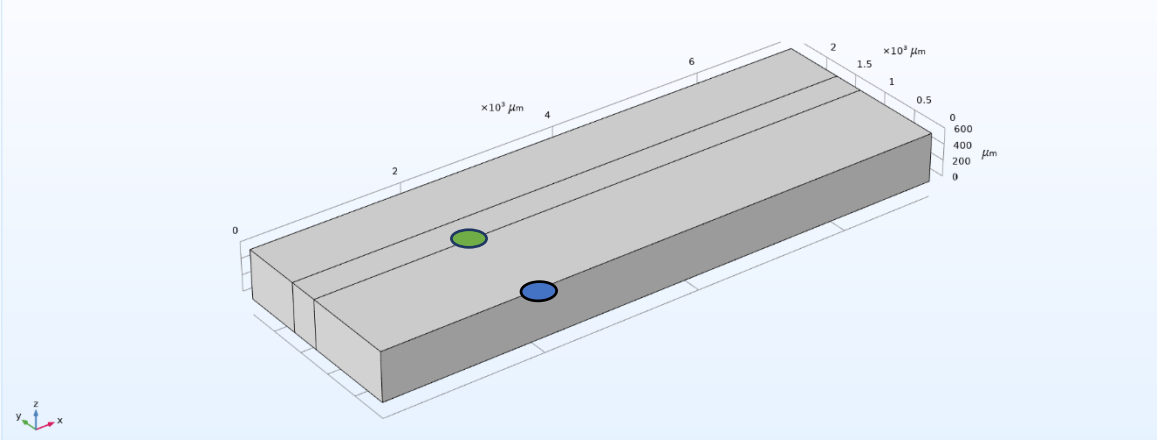

Figure 5.13: Schematic of chosen reference points

Blue circle represents point number 9

Green circle represents point number 10

These two points were taken as reference for plotting the tempetarure variation wrt time and thermal stress variation w.r.t time one dimensionally. The following results

Will show that variation at different scanning speeds for pulse power 1J.

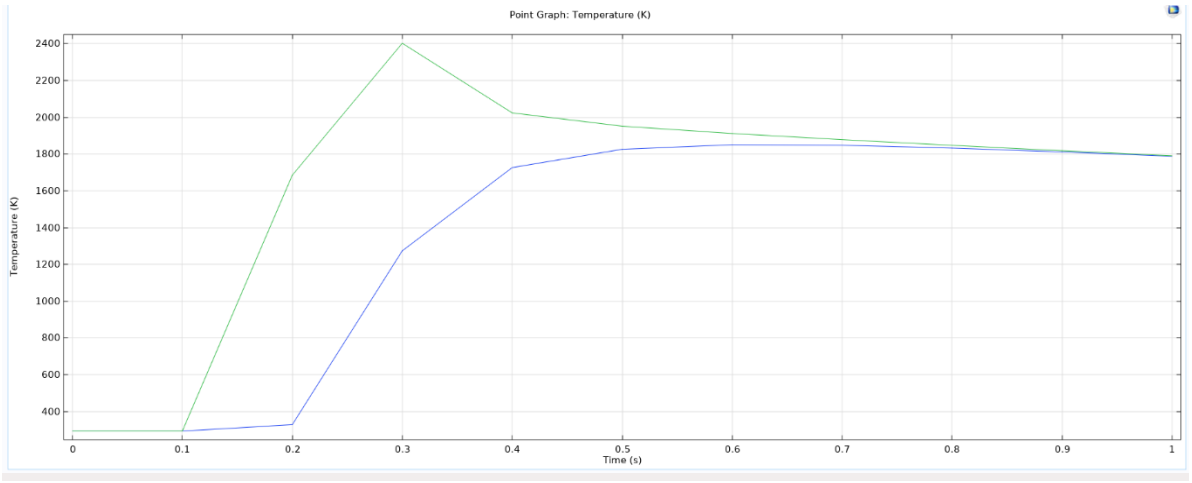

Figure.5.14.1 1-D Temperature plot when the pulse power is 1J and scanning speed is 25mm/s

The above plot shows the temperature distribution of those selected points. It is observed that the temperature increases reaching to a maximum point and gradually decreases. It is also noticed that point 9 always maintained at lower temperature than point 10.

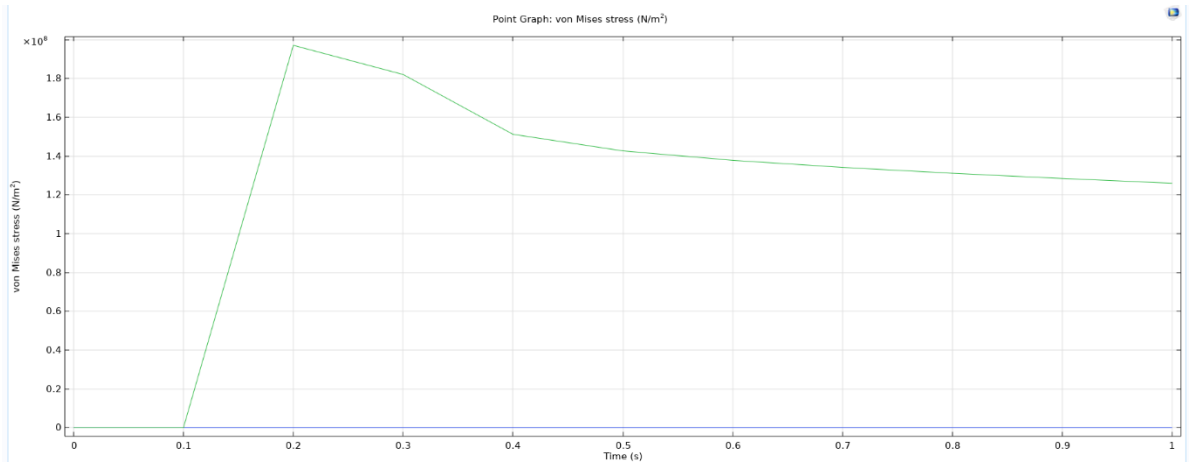

Figure.5.14.2 1-D Thermal stress plot when the pulse power is 1J and scanning speed is 25mm/s

The above plot is 1D thermal stress plot for selected reference points in which thermal stress is taken on y axis and time on x axis. The point 9 is subjected to constant thermal stress whereas the point 10 is subjected to thermal which is varying w.r.t time. For point the thermal stress reached to a maximum state and keeps on decreasing gradually w.r.t. time.

CONCLUSION

- In this study temperature and thermal stress distribution of TITANIUM GRADE 9 was predicted and presented using COMSOL MULTIPHYSICS,
- While modelling the simulation of SLS process by using COMSOL Multiphysics Software, the maximum temperature and the maximum thermal stresses of the melt pool were analysed and represented.
- The effect of laser parameters like pulse power and scanning speed were studied.
- The heat source resulted in melt pool peak temperature and maximum thermal stress were simulated and predicted successfully.
- Taking pulse power on X-axis and temperature on Y-axis keeping laser scanning speed i.e., 25mm/s as constant parameter, we plotted the graph and it is observed that the temperature decreases w.r.t time. The maximum thermal stress obtained as 2.3GPa at pulse power of 4J.
- Taking the time on X-axis and thermal stress on Y-axis, we plotted the graph for different laser scanning speeds considering pulse power of 1J as constant. It is observed that thermal stresses also decreases w.r.t time. It is noticed that the maximum thermal stress was obtained as 1.1GPa in the case of pulse power of 1J with scanning speed as 25mm/s.
- Distribution of maximum temperature and maximum thermal stress at the scanning speed of 10mm/s were shown in the pie chart. It is observed that the maximum percentage of distribution of temperature and thermal stress were given by 31% and 33% respectively.
- The maximum temperature and maximum thermal stress for the scanning speed of 10mm/s were occured at pulse power of 4J and 3J respectively.
- The peak temperature is obtained at 4J with scanning speed of 15mm/s is about 17000 K and the maximum stress is obtained at a scanning speed of 20mm/s with a pulse power of 4J is about 2.4 Gpa.
- Along with Temperature distribution and thermal stress distribution principal stress distribution, temperature gradients and volumetric strain were studied and analysed in this research.
- The Gaussian heat source predicted melt pool characteristics and it was observed that optimal pulse power and laser scanning speeds are 1J and 25mm/s respectively.

REFERENCES

[1] Akash Aggarwal, Sushil Patel and Aravind Kumar, Selective Laser Melting of 316L Stainless Steel: Physics of Melting Mode Transition and Its Influence on Microstructural and Mechanical Behavior, Additive manufacturing: validation and control, published:12 December,2018.

[2] Akash Aggarwal, Ashish Kumar Mishra1, Arvind Kumar1 and Niraj Sinha1, Identification of a suitable volumetric heat source for modelling of selective laser melting of Ti6Al4V powder using numerical and experimental validation approach, Accepted: 20 August 2018.

[3] Yadaiah N, Bag S (2014) Development of egg-configuration heat source model in numerical simulation of autogenous fusion welding process. Int J Therm Sci 86:125–138.

[4] Fan Z, Liou F (2012) Numerical modeling of the additive manufacturing (AM) processes of titanium alloy. Nurul Amin AKM (ed) Titanium alloys - towards achieving enhanced properties for diversified applications.

[5]Olawale-Computational modelling of laser additive manufactured (LAM) Titanium alloy grade 5

[6] X. Wu, J. Liang, J. Mei, C. Mitchell, P. Goodwin, and W. Voice, "Microstructures of Laser Deposited Ti- 6Al-4V," Materials and Design, vol. 25A, pp. 137–144, (2004).

[7]John Kummailil, Carmine Sammarco, David kinner, Christopher A. Brown, "Effect of Select LENS Processing Parameters on the Deposition of Ti-6Al- 4V." (2005).

[8]S. Bontha, N. W. Klingbeil, P. A. Kobryn, and H. L. Fraser, "Thermal Process Maps for Predicting Solidification Microstructure in Laser Fabrication of Thin-Wall Structures," Journal of Materials Processing Technology, vol. 178, no. 1–3, pp. 135–142, (2006).

[9]K.-H. Leitz, P. Singer, A. Plankensteiner, B. Tabernig, H. Kestler, L.S. Sigl -Thermo-Fluiddynamical Modelling of Laser Beam-Matter Interaction in Selective Laser Melting- Published in Nov. 2016

[10]Babis Schoinochoritis, Dimitrios Chantzis, Konstantinos Salonitis-Simulation of metallic powder bed additive manufacturing processes with the finite element method - publishes in jan 28,2015

[11]F.-J. Gürtler, M. Karg, K.-H. Leitz, M. Schmidt: Simulation of laser beam melting of steel powders using the three-dimensional volume of fluid method, Physics Procedia, 41, 874-879 (2013)

[12]K.-H. Leitz, P. Singer, A. Plankensteiner, B. Tabernig, H. Kestler, L.S. Sigl, Multi-Physical Simulation of Selective Laser Melting, Metal Powder Report (2016) - in press.